

We thank the referee and the editor for the helpful comments. Please find our responses below.

### 1) Comment

First of all, the authors have done a good job answering the comments. The responses are clear and addressed the issues.

Still, there is one thing I do not understand. The authors stated that they cannot find DMS values for the year 2007. However, in Müller et al. (2010), there are DMS values reported for May to June 2007 measured at the Cape Verde Atmospheric Observatory (CVAO). As mentioned in my former response, since 2006 DMS concentrations are permanently measured there (see Carpenter et al., 2010). This station is operated by the National Centre for Atmospheric Science, Department of Chemistry, University of York. As two of the Co-authors are working at this University and one also at the National Centre for Atmospheric Science, I do not understand why it is not possible to get data access. Are there lacks in the measurements for 2007? Please clarify this.

Overall, if this issue is clarified, the paper is suitable for publication in ACP.

**Response:** We have spoken to the P.I. of CVAO (Lucy Carpenter). Unfortunately, she informed us that the DMS data is not yet available to be shared as it still requires further processing and quality control.

**Changes in the manuscript:** No changes.

### 2) Comment

In addition, the expressions of multiphase or aqueous reactions somewhere in the manuscript are not very clear to me. Specifically, at Page 5, Line 24-28, are DMS, DMSO, MSIA and MSA gaseous or liquid species? Are their reactions with O<sub>3</sub>(aq) and OH(aq) the same as those aqueous-phase reactions shown in Table 1? The issue is that an index of (aq) is used for DMS, DMSO, MSIA and MSA in Table 1, but not in the text.

**Response:** The multiphase reaction starts with the uptake of gas-phase sulfur species into the cloud droplets and aerosols, followed by the reaction in the aqueous-phase of this sulfur species with the aqueous-phase oxidants OH<sub>(aq)</sub> and O<sub>3(aq)</sub>. The aqueous-phase rate constant in Table 1 is for the aqueous part of the multiphase reaction. Therefore, in the updated manuscript, we denote multiphase reaction in the form of X<sub>(g)</sub>+OH<sub>(aq)</sub> but rate constant for the aqueous-phase reaction in the form of X<sub>(aq)</sub>+OH<sub>(aq)</sub>.

#### Changes in the manuscript:

- Page 5, Line 24-28: change into:

For the multiphase reactions DMS<sub>(g)</sub> + O<sub>3(aq)</sub>, DMSO<sub>(g)</sub> + OH<sub>(aq)</sub>, MSIA<sub>(g)</sub> + OH<sub>(aq)</sub>, MSIA<sub>(g)</sub> + O<sub>3(aq)</sub> and MSA<sub>(g)</sub> + OH<sub>(aq)</sub> in cloud droplets and aerosols, we assume a first-order loss of the gas-phase sulfur species, following the parameterization described in Ammann et al. (2013) and Chen et al. (2017):

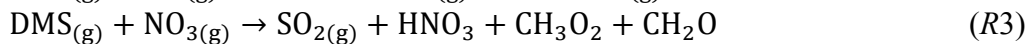
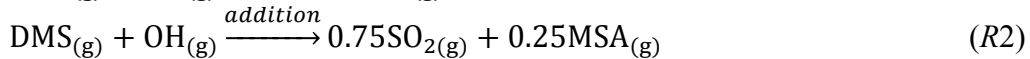
$$\frac{d[X_{(g)}]}{dt} = -\frac{c\gamma}{4} A[X_{(g)}] , \quad (E4)$$

- Page 6, Line 12: add:

Gas-phase sulfur species taken up by aerosols and cloud droplets will be oxidized in the aqueous phase.

Change “ $k_{X+Y}$  is the aqueous-phase reaction rate coefficient between X and Y ( $M^{-1} s^{-1}$ ), as summarized in Table 1.” into “ $k_{X+Y}$  is the aqueous-phase reaction rate coefficient between aqueous-phase X and Y ( $M^{-1} s^{-1}$ ), as summarized in Table 1.”

- Page 4, Line 22-29: specify gas phase oxidation of DMS.



# DMS oxidation and sulfur aerosol formation in the marine troposphere: a focus on reactive halogen and multiphase chemistry

Qianjie Chen<sup>1\*</sup>, Tomás Sherwen<sup>2</sup>, Mathew Evans<sup>2,3</sup>, and Becky Alexander<sup>1</sup>

<sup>1</sup>Department of Atmospheric Sciences, University of Washington, Seattle, WA, USA

<sup>2</sup>Wolfson Atmospheric Chemistry Laboratories, Department of Chemistry, University of York, York, UK

<sup>3</sup>National Centre for Atmospheric Science (NCAS), University of York, York, UK

\*Now at Department of Chemistry, University of Michigan, Ann Arbor, MI, USA

Correspondence to: Becky Alexander (beckya@atmos.washington.edu)

**Abstract.** The oxidation of dimethyl sulfide (DMS) in the troposphere and subsequent chemical conversion into sulfur dioxide ( $\text{SO}_2$ ) and methane sulfonic acid (MSA) are key processes for the formation and growth of sulfur-containing aerosol and cloud condensation nuclei (CCN), but is highly simplified in large-scale models of the atmosphere. In this study, we implement a series of gas-phase and multiphase sulfur oxidation mechanisms into the GEOS-Chem global chemical transport model, including two important intermediates dimethyl sulfoxide (DMSO) and methane sulphinic acid (MSIA), to investigate the sulfur cycle in the global marine troposphere. We found that DMS is mainly oxidized in the gas phase by OH (66%),  $\text{NO}_3$  (16%) and  $\text{BrO}$  (12%) globally.  $\text{DMS} + \text{BrO}$  is important for the model's ability to reproduce the observed seasonality of surface DMS mixing ratio in the Southern Hemisphere. MSA is mainly produced from multiphase oxidation of MSIA by  $\text{OH}_{(\text{aq})}$  (66%) and  $\text{O}_3_{(\text{aq})}$  (30%) in cloud droplets and aerosols. Aqueous-phase reaction with OH accounts for only 12% of MSA removal globally and a higher MSA removal rate is needed to reproduce observations of MSA/nss $\text{SO}_4^{2-}$  ratio. The modeled conversion yield of DMS into  $\text{SO}_2$  and MSA is 75% and 15%, respectively, compared to 91% and 9% in the standard model run that includes only gas-phase oxidation of DMS by OH and  $\text{NO}_3$ . The remaining 10% of DMS is lost via deposition of intermediates DMSO and MSIA. The largest uncertainties for modeling sulfur chemistry in the marine boundary layer (MBL) are unknown concentrations of reactive halogens ( $\text{BrO}$  and Cl) and  $\text{OH}_{(\text{aq})}$  concentrations in cloud droplets and aerosols. To reduce uncertainties in MBL sulfur chemistry, we should prioritize observations of reactive halogens and  $\text{OH}_{(\text{aq})}$ .

## 25 1 Introduction

The biogenic emission of dimethyl sulfide (DMS:  $\text{CH}_3\text{SCH}_3$ ) from the ocean is the largest natural sulfur source to the atmosphere (Andreae, 1990). After emission, DMS is mainly oxidized in the troposphere, with a lifetime against oxidation of 1-2 days (Chin et al., 1996; Boucher et al., 2003; Breider et al., 2010). The oxidation of DMS and subsequent formation of other sulfur species such as sulfuric acid ( $\text{H}_2\text{SO}_4$ ) and methane sulfonic acid (MSA:  $\text{CH}_3\text{SO}_3\text{H}$ ) are crucial for the formation 30 and evolution of natural aerosols and clouds in the marine boundary layer (MBL) and thus have profound climate

implications (Charlson et al., 1987; von Glasow and Crutzen, 2004; Thomas et al., 2010). In particular, Carslaw et al. (2013) pointed out that natural aerosols such as those that originate from DMS oxidation account for the largest uncertainty of aerosol radiative forcing in climate models.

5 The atmospheric fate of DMS determines the extent to which DMS affects our climate system. Production of  $\text{H}_2\text{SO}_4$  and MSA from gas-phase oxidation of DMS-derived products can result in nucleation of new particles under favorable conditions (Kulmala et al., 2000; Chen et al., 2015), with implications for aerosol and CCN number concentrations. Sulfate and MSA formed in the aqueous phase will not result in new particle formation, but will impact the aerosol size distribution with implications for cloud microphysical properties (Kreidenweis and Seinfeld, 1988; Kaufman and Tanre, 1994). The  
10 oxidation mechanisms of DMS and subsequent formation of sulfate and MSA are, however, very complicated and still not well understood even after decades of research (Ravishankara et al., 1997; Barnes et al., 2006; Hoffmann et al., 2016). Large-scale models of atmospheric chemistry typically contain very simplified DMS chemistry, and often ignore potentially important reaction intermediates. Most of these models include oxidation of DMS by OH and  $\text{NO}_3$  radicals, directly  
15 producing  $\text{SO}_2$  and MSA, and ignore the formation of dimethyl sulfoxide (DMSO:  $\text{CH}_3\text{SOCH}_3$ ) and methane sulphinic acid (MSIA:  $\text{CH}_3\text{SO}_2\text{H}$ ) intermediates (Chin et al., 1996; 2000; Gondwe et al., 2003; 2004; Berglen et al., 2004; Kloster et al., 2006). Nevertheless, previous large-scale modeling studies suggested that BrO could be an important sink for DMS globally  
20 (up to 30%), especially in the remote MBL where BrO mixing ratios can reach ppt levels (Boucher et al., 2003; von Glasow et al., 2004; Breider et al., 2010; Khan et al., 2016). Other oxidants that may be important for DMS oxidation include Cl radicals in the gas phase (von Glasow and Crutzen, 2004; Hoffmann et al., 2016) and  $\text{O}_3$  in the gas and aqueous phase (Boucher et al., 2003; Hoffmann et al., 2016).

Some large-scale models have simulated the formation of the DMSO intermediate from DMS oxidation (Pham et al., 1995; Cosme et al., 2002; von Glasow et al., 2004; Castebrunet et al., 2009), which is important as DMSO is highly water soluble (Henry's law constant ( $H_{\text{DMSO}}$ ) on the order of  $10^7 \text{ M atm}^{-1}$ ) and can undergo dry and wet deposition in addition to gas- and  
25 aqueous-phase oxidation to MSA or  $\text{SO}_2$  (Lee and Zhou, 1994; Campolongo et al., 1999; Barnes et al., 2006; Zhu et al., 2006; Hoffmann et al., 2016). In the cloud-free MBL, DMSO is mainly produced by  $\text{DMS} + \text{BrO}$  and  $\text{DMS} + \text{OH}_{(\text{g})}$  via the addition channel and is oxidized by OH in the gas phase. In the cloudy MBL, DMSO is mainly produced via  $\text{DMS} + \text{O}_{3(\text{aq})}$  and oxidized via  $\text{DMSO} + \text{OH}_{(\text{aq})}$  in the aqueous phase (Hoffmann et al., 2016). Knowledge about aqueous-phase concentrations  
30 of OH in cloud droplets and aerosols is still very limited. Modeled  $\text{OH}_{(\text{aq})}$  concentrations are on the order of  $10^{-14}$ - $10^{-12} \text{ M}$  (Jacob, 1986; Matthijsen et al., 1995; Jacob et al., 1989; Herrmann et al., 2000). However, recent observations of  $\text{OH}_{(\text{aq})}$ , which are derived from the concentrations of dissolved organic compounds, are about two orders of magnitude lower ( $10^{-16}$ - $10^{-14} \text{ M}$ ) (Arakaki et al., 2013; Kaur and Anastasio, 2017). In addition to aqueous-phase oxidation of DMSO by  $\text{OH}_{(\text{aq})}$ , a box modeling study by Zhu et al. (2006) suggested that  $\text{SO}_4^-$  and  $\text{Cl}_2^-$  could contribute to 34% and 10% of DMSO oxidation in the aqueous phase, respectively, with  $\text{SO}_4^-$  and  $\text{Cl}_2^-$  concentrations of  $1 \times 10^{-12} \text{ M}$  and  $1 \times 10^{-11} \text{ M}$  (Herrmann et al., 2000),

respectively. It should be noted that  $\text{OH}_{(\text{aq})}$ ,  $\text{SO}_4^{2-}$  and  $\text{Cl}_2^-$  concentrations are poorly known and the contribution of these species to DMSO oxidation will depend on their concentrations.

MSIA is generally not included in large-scale models, though it has been considered in some one-dimensional or box models (Lucas and Prinn, 2002; von Glasow and Crutzen, 2004; Zhu et al., 2006; Hoffmann et al., 2016). The Henry's law constant of MSIA has not been measured directly but is thought to be larger than that of DMSO and smaller than that of MSA, on the order of  $10^8 \text{ M atm}^{-1}$  (Barnes et al., 2006). MSIA is mainly produced from oxidation of DMSO by OH in both the gas and aqueous phase, and removed via further oxidation by OH and  $\text{O}_3$  in both the gas and aqueous phase and  $\text{Cl}_2^-$  in the aqueous phase (von Glasow and Crutzen, 2004; Zhu et al., 2006; Barnes et al., 2006; Hoffmann et al., 2016). Only oxidation of MSIA by OH in the gas phase produces  $\text{SO}_2$ , all other pathways lead to MSA formation. The contribution of each pathway towards MSIA oxidation depends on the concentration of each oxidant. Zhu et al. (2006) suggested  $\text{Cl}_2^-$  is more important than  $\text{OH}_{(\text{aq})}$  for MSIA oxidation in the aqueous phase when assuming a  $\text{Cl}_2^-$  concentration of  $1 \times 10^{-11} \text{ M}$  (Herrmann et al., 2000), while Hoffmann et al. (2016) suggested the opposite with a lower  $\text{Cl}_2^-$  concentration ( $1.5 \times 10^{-12} \text{ M}$ ).

The only source of MSA in the marine troposphere is from oxidation of DMS emitted from the marine biosphere. It thus contains information on both DMS emission flux and chemistry. It has been proposed as an ice-core proxy for sea ice extent in past climates, as a result of melting sea ice releasing nutrients to stimulate phytoplankton growth to produce DMS (Curran et al., 2003; Abram et al., 2010). Other factors such as oxidation mechanisms of DMS and atmospheric circulation can also affect MSA abundance in ice core records (Becagli et al., 2009; Hezel et al., 2011). As DMS is the dominant sulfur source of both MSA and non-sea-salt sulfate ( $\text{nssSO}_4^{2-}$ ) in the remote marine troposphere, the MSA/nss $\text{SO}_4^{2-}$  molar ratio there reflects sulfur chemistry. In addition, the MSA/nss $\text{SO}_4^{2-}$  molar ratio has often been used as a measure of marine biogenic contribution to total atmospheric sulfate formation, as  $\text{nssSO}_4^{2-}$  has both anthropogenic and natural origins while MSA is generally considered to have a predominant natural origin (Andreae et al., 1999; Savoie et al., 2002; Gondwe et al., 2004). MSA is very water soluble, with a Henry's law constant on the order of  $10^9 \text{ M atm}^{-1}$  (Campolongo et al., 1999), and is mainly removed from the atmosphere via wet and dry deposition with a lifetime of about a week (Pham et al., 1995; Chin et al., 1996; 2000; Cosme et al., 2002; Hezel et al., 2011). One-dimensional modeling studies by Zhu et al. (2006) and von Glasow and Crutzen (2004) suggested that the oxidation of MSA by  $\text{OH}_{(\text{aq})}$  in the aqueous phase to form  $\text{SO}_4^{2-}$  in the MBL could also be a significant loss process of MSA (3-27%) (Zhu et al., 2006; von Glasow and Crutzen, 2004), while a box modeling study by Hoffmann et al. (2016) found it negligible (2%). The different conclusions regarding the role of reaction of MSA with  $\text{OH}_{(\text{aq})}$  is due to different assumptions regarding  $\text{OH}_{(\text{aq})}$  concentrations, which is highly uncertain.

In this study, we expand upon the current simplified DMS chemistry in a global chemical transport model GEOS-Chem, including the DMSO and MSIA intermediates. We investigate the role of gas-phase and multiphase oxidation of DMS, DMSO, MSIA and MSA for determining their spatial distribution, seasonality, and lifetime and the implications for the

MBL and global sulfur budget. Observations of DMS mixing ratios from 4 locations and MSA/nssSO<sub>4</sub><sup>2-</sup> ratios from 23 locations around the globe obtained from previous studies are used to assess the performance of model. We conclude with recommendations for future laboratory experiments and field campaigns, and recommendations for sulfur chemistry that should be included in large-scale models of atmospheric chemistry and climate.

## 5 2 GEOS-Chem model

In this study, we use a global 3-D chemical transport model GEOS-Chem v9-02 (<http://www.geos-chem.org/>), which is driven by assimilated meteorological data from the NASA Goddard Earth Observing System (GEOS-5, <http://gmao.gsfc.nasa.gov>). It contains detailed HO<sub>x</sub>-NO<sub>x</sub>-VOC-ozone-BrO<sub>x</sub> tropospheric chemistry originally described in Bey et al. (2001), with updated BrO<sub>x</sub> and sulfate chemistry described in Parrella et al. (2011), Schmidt et al. (2016) and Chen et al. (2017). The sulfate-nitrate-ammonium aerosol simulation is fully coupled to gas-phase chemistry (Park et al., 2004), with aerosol thermodynamics described in Pye et al. (2009). The sea salt aerosol simulation is described in Jaeglé et al. (2011) and bulk cloud water pH is calculated as described in Alexander et al. (2012). The model contains detailed deposition schemes for both gas species and aerosols (Liu et al., 2001; Amos et al., 2012; Zhang et al., 2001; Wang et al., 1998). All simulations are performed at 4°×5° horizontal resolution and 47 vertical levels up to 0.01 hPa (≈81 km) after a model spin up of one year. The vertical layer thickness ranges from 120-150 m for the first 12 layers to 200-800 m for the 13<sup>th</sup>-27<sup>th</sup> layers and >1000 m for the rest ([http://acmg.seas.harvard.edu/geos/doc/archive/man.v9-01-02/appendix\\_3.html#A3.5.2](http://acmg.seas.harvard.edu/geos/doc/archive/man.v9-01-02/appendix_3.html#A3.5.2)). Year 2007 is chosen as a reference year to be consistent with Schmidt et al. (2016) and Chen et al. (2017). DMS emission flux from the ocean ( $F$ ) is parameterized following Lana et al. (2011):  $F = k_T C_w$ , where gas transfer velocity  $k_T$  (m s<sup>-1</sup>) is a function of sea surface temperature and wind speed and  $C_w$  (mol m<sup>-3</sup>) is the DMS concentrations in sea water obtained from Lana et al. (2011). In a sensitivity simulation, we used  $C_w$  from Kettle et al. (1999).

The standard model contains only three gas-phase DMS oxidation pathways in the original version, which produces SO<sub>2</sub> and MSA directly (R1-R3), following Chin et al. (1996) with updated reaction rate coefficients from Burkholder et al. (2015):



30 The yields of SO<sub>2</sub> and MSA for the addition channel of the gas-phase DMS+OH reaction are originally from Chatfield and Crutzen (1990), who made simplified assumptions in their 2-D model based on previous laboratory experiments and modeling studies. It should be noted that only gas-phase chemistry was considered when they made the assumptions of the

Qianjie Chen 9/5/18 10:39 AM

**Deleted:** DMS

Qianjie Chen 9/5/18 10:39 AM

**Deleted:** OH

Qianjie Chen 9/5/18 10:39 AM

**Deleted:** DMS

Qianjie Chen 9/5/18 10:40 AM

**Deleted:** OH

Qianjie Chen 9/5/18 10:41 AM

**Deleted:** MSA

Qianjie Chen 9/5/18 10:39 AM

**Deleted:** DMS

yields of  $\text{SO}_2$  and MSA, which might not represent the real atmosphere as multiphase chemistry has been suggested to be the biggest source of MSA in the atmosphere (Zhu et al., 2006; Hoffmann et al., 2016).

We add the DMSO and MSIA intermediates as two new advected chemical tracers, which undergo chemical production and loss, transport and deposition in the model. We add 12 new chemical reactions in the model, including gas-phase oxidation of DMS by OH (addition channel, modified to produce DMSO instead of MSA),  $\text{BrO}$ ,  $\text{Cl}$  and  $\text{O}_3$ , multiphase oxidation of DMS by  $\text{O}_3$ , both gas-phase and multiphase oxidation of DMSO by OH, both gas-phase and multiphase oxidation of MSIA by OH and  $\text{O}_3$ , and multiphase oxidation of MSA by OH, as shown in Table 1. The rate coefficients for all gas-phase sulfur reactions are obtained from the most recent JPL report (Burkholder et al., 2015), except for  $\text{MSIA}_{(g)} + \text{O}_3(g)$  (Lucas and Prinn, 2002; von Glasow and Crutzen, 2004). The sulfur product yields for gas-phase reactions are obtained from various laboratory and modeling studies as indicated in Table 1. Product yields of 0.6 for  $\text{SO}_2$  and 0.4 for DMSO have been commonly used in global models (Pham et al., 1995; Cosme et al., 2002; Spracklen et al., 2005; Breider et al., 2010) based on experiments described in Turnipseed et al. (1996) and Hynes et al. (1993). All oxidants ( $\text{OH}$ ,  $\text{O}_3$ ,  $\text{H}_2\text{O}_2$ ,  $\text{BrO}$ ,  $\text{HOBr}$ ) are simulated in the full chemistry scheme, except for  $\text{Cl}$  radicals. We used monthly mean  $\text{Cl}$  mixing ratios from Sherwen et al. (2016), which considered  $\text{Cl-Br-I}$  coupling but did not include chlorine production on sea salt aerosols that was suggested to be the largest tropospheric chlorine source in Schmidt et al. (2016). We imposed a diurnal variation of  $\text{Cl}$  abundances based on solar zenith angle, similar to the offline simulation of OH abundances in GEOS-Chem (Fisher et al., 2017). The global distributions of tropospheric annual-mean concentrations of  $\text{BrO}$ ,  $\text{Cl}$ ,  $\text{OH}$  and  $\text{O}_3$  are shown in Fig. 12. The high  $\text{BrO}$  abundances over subtropics and polar regions are due to low deposition fluxes of reactive bromine (Schmidt et al., 2016) and the high  $\text{BrO}$  abundance over Southern Ocean is due to its source from sea salt debromination (Chen et al., 2017). The high  $\text{Cl}$  abundance over coastal regions in the Northern Hemisphere is due to heterogeneous uptake of  $\text{N}_2\text{O}_5$  on sea salt aerosols to produce reactive chlorine (Sherwen et al., 2017).

Qianjie Chen 8/29/18 11:30 AM

Deleted: ( $k_{\text{MSIA}+\text{O}_3(g)}$ )

For the multiphase reactions  $\text{DMS}_{(g)} + \text{O}_3(aq)$ ,  $\text{DMSO}_{(g)} + \text{OH}_{(aq)}$ ,  $\text{MSIA}_{(g)} + \text{OH}_{(aq)}$ ,  $\text{MSIA}_{(g)} + \text{O}_3(aq)$  and  $\text{MSA}_{(g)} + \text{OH}_{(aq)}$  in cloud droplets and aerosols, we assume a first-order loss of the gas-phase sulfur species, following the parameterization described in Ammann et al. (2013) and Chen et al. (2017):

$$\frac{d[\text{X}_{(g)}]}{dt} = -\frac{c\gamma}{4} A[\text{X}_{(g)}], \quad (E4)$$

where  $\text{X}$  represents DMS, DMSO, MSIA or MSA;  $c$  is the average thermal velocity of  $\text{X}$  ( $\text{m s}^{-1}$ );  $A$  ( $\text{m}^2 \text{ m}^{-3}$ ) is the total surface area concentration of aerosols or cloud droplets;  $\gamma$  (unitless) is the reactive uptake coefficient of  $\text{X}$  that involves gas diffusion ( $\gamma_d$ ), mass accommodation ( $\alpha_b$ ) and chemical reaction ( $\Gamma_b$ ) in the aerosols or cloud droplets, as calculated in E5-E7.

$$\frac{1}{\gamma} = \frac{1}{\gamma_d} + \frac{1}{\alpha_b} + \frac{1}{\Gamma_b} \quad (E5)$$

$$\gamma_d = \frac{4D_g}{cr} \quad (E6)$$

$$\Gamma_b = \frac{4H_XRT\sqrt{D_{lX}k_{X+Y}[Y]f_r}}{c} \quad (E7)$$

where  $r$  is radius for aerosols or cloud droplets (m);  $D_g$  is the gas phase diffusion coefficient of X ( $\text{m}^2 \text{ s}^{-1}$ ), calculated as a function of air temperature and air density following Chen et al. (2017).  $H_X$  and  $D_l$  are the Henry's law constant ( $\text{M atm}^{-1}$ ) and liquid phase diffusion coefficient ( $\text{m}^2 \text{ s}^{-1}$ ) of X, which are summarized in Table 2;  $R$  ( $=8.31 \times 10^{-2} \text{ L bar mol}^{-1} \text{ K}^{-1}$ ) is the universal gas constant.  $T$  is air temperature (K);  $[Y]$  ( $=[\text{OH}_{(\text{aq})}]$  or  $[\text{O}_3_{(\text{aq})}]$ ) is the aqueous phase concentration of the oxidant in aerosols or cloud droplets (M), where  $[\text{O}_3_{(\text{aq})}]$  is calculated assuming gas-liquid equilibrium and  $[\text{OH}_{(\text{aq})}]$  is calculated following Jacob (2005) ( $[\text{OH}_{(\text{aq})}] = \beta[\text{OH}_{(\text{g})}]$ ,  $\beta = 1 \times 10^{-19} \text{ M cm}^3 \text{ molecule}^{-1}$ ). This is about two orders of magnitude higher than  $[\text{OH}_{(\text{aq})}]$  calculated indirectly from dissolved organic compound observations in Arakaki et al. (2013) and Kaur and Anastasio (2017). Thus, we conduct a sensitivity simulation reducing  $[\text{OH}_{(\text{aq})}]$  in cloud droplets and aerosols by two orders of magnitude (Table 3). We conduct another sensitivity simulation by reducing the  $[\text{OH}_{(\text{aq})}]$  in aerosols only by a factor of 20 (Herrmann et al., 2010) and found negligible changes (<2%) in the global sulfur burden. Gas-phase sulfur species taken up by aerosols and cloud droplets will be oxidized in the aqueous phase.  $k_{X+Y}$  is the aqueous-phase reaction rate coefficient between aqueous-phase X and Y ( $\text{M}^{-1} \text{ s}^{-1}$ ), as summarized in Table 1.  $f_r$  ( $=\coth(r/l) - l/r$ ) is the reacto-diffusive correction term, which compares the radius of aerosols or cloud droplets ( $r$ ) with the reacto-diffusive length scale of the reaction ( $l = \sqrt{D_l/(k_{X+Y}[Y])}$ ) (Ammann et al., 2013). The mass accommodation coefficients ( $\alpha_b$ ) of DMS, DMSO, MSIA and MSA are given in Table 2.

Twelve model simulations were performed in order to investigate the importance of individual reactions for MBL sulfur chemistry and are described in Table 3. These simulations were designed to explore the role of DMS chemistry versus emissions for the DMS budget, and the importance of gas-phase reactive halogen chemistry and multiphase chemistry for all sulfur-containing compounds.

### 3 Results and Discussion

#### 3.1 DMS budget

Figure 1 shows the global sulfur budgets for the model run including DMSO and MSIA intermediates and all 12 new reactions ( $R_{\text{all}}$ ). The DMS emission flux from the ocean to the atmosphere ( $F_{\text{DMS}}$ ) is  $22 \text{ Tg S yr}^{-1}$ , which is similar to that ( $24 \text{ Tg S yr}^{-1}$ ) reported in Hezel et al. (2011) and within the range ( $11\text{-}28 \text{ Tg S yr}^{-1}$ ) reported in the literature (Spracklen et al., 2005 and reference therein).  $F_{\text{DMS}}$  is  $18 \text{ Tg S yr}^{-1}$  when using sea surface DMS concentrations from Kettle et al. (1999). The tropospheric burden of DMS is  $74 \text{ Gg S}$ , which is within the range of  $20\text{-}150 \text{ Gg S}$  reported in Faloona et al. (2009), and is 40% lower than the standard model run ( $R_{\text{std}}$ ). The lifetime of DMS is 1.2 days in  $R_{\text{all}}$ , compared to 2.1 days in  $R_{\text{std}}$ . Surface

DMS mixing ratios are highest over Southern Ocean ( $\approx 400$  ppt) (Fig. 2a) where DMS emissions are highest during summer (Lana et al., 2011) and DMS chemical destruction is small due to low OH abundance at high latitudes (DMS lifetime of 2-5 days over Southern Ocean). DMS mainly resides in the lower troposphere, with 86% of the tropospheric burden below 2 km. DMS is mainly oxidized in the gas phase by OH (37% via abstraction channel and 29% via addition channel), followed by  $5$   $\text{NO}_3$  (16%). The global contribution of OH and  $\text{NO}_3$  to DMS oxidation from previous studies is 50%-70% and 20%-30%, respectively, depending mainly on which other oxidants are included (Boucher et al., 2003; Berglen et al., 2004; Breider et al., 2010; Khan et al., 2016). The oxidation of DMS by OH occurs mainly during daytime while oxidation by  $\text{NO}_3$  occurs mainly at night due to low nighttime OH production and rapid photolysis of  $\text{NO}_3$  during daytime. Fig. 3 shows the global, 10 annual mean distribution of the fractional importance of different DMS oxidation pathways. The relative importance of OH for the oxidation of DMS ( $f_{\text{H}_2\text{O}|\text{DMS}}$ ) is typically greater than 50% over the oceans. The relative importance of  $\text{NO}_3$  for the oxidation of DMS ( $f_{\text{NO}_3|\text{DMS}}$ ) is typically low over the remote oceans (<10%), but high over the continents and coastal regions (>40%) where  $\text{NO}_x$  emissions are highest. It should be noted, however, that DMS abundance is low over continents (Fig. 2a).

15 The relative importance of  $\text{BrO}$  oxidation of DMS ( $f_{\text{BrO}|\text{DMS}}$ ) is 12% (global, annual mean), which is within the range suggested by Khan et al. (2016) (8%) and Breider et al. (2010) (16%).  $f_{\text{BrO}|\text{DMS}}$  is highest (>30%) over the Southern Ocean and Antarctica, especially during winter, due to high  $\text{BrO}$  (up to 0.5 ppt) and low OH and  $\text{NO}_3$  abundance. The main uncertainty of the importance of  $\text{BrO}$  for DMS oxidation resides in the tropospheric  $\text{BrO}$  abundance, which is rarely measured and is still not well quantified in global models (von Glasow et al., 2004; Simpson et al., 2015). The  $\text{BrO}$  in our 20 model generally underestimates satellite observations, especially over mid- and high-latitudes (Chen et al., 2017), suggesting that our modeled estimate of the importance of DMS+ $\text{BrO}$  may be biased low. In order to quantify the contribution of  $\text{BrO}$  to DMS oxidation, we need to better quantify the  $\text{BrO}$  abundance through both observation and model development.

25 The fractional contribution of Cl to DMS oxidation ( $f_{\text{Cl}|\text{DMS}}$ ) is 4% globally and generally less than 10% everywhere.  $f_{\text{Cl}|\text{DMS}}$  increases to 28% in a sensitivity run increasing Cl mixing ratios by an order of magnitude. In comparison, von Glasow and Crutzen (2004) calculate that about 8% of DMS is oxidized by Cl in the cloud-free MBL during summer in a 1-D model. Hoffmann et al. (2016) estimated that about 18% of DMS is oxidized by Cl under typical MBL conditions in a box model. Both studies used the same  $k_{\text{DMS+Cl}}$  as in our study, but Cl concentrations were not reported in either study. The 30 annual-mean tropospheric Cl concentration used in this study is  $1.1 \times 10^3$  atoms  $\text{cm}^{-3}$ , which is similar to that ( $1.3 \times 10^3$  atoms  $\text{cm}^{-3}$ ) in another recent 3-D modeling study (Hossaini et al., 2016). As suggested by Sherwen et al. (2016), Cl concentration could be underestimated in our study, due at least in part to the missing chlorine source from sea salt aerosols and anthropogenic chloride emissions. The largest uncertainty for the importance of Cl for the oxidation of DMS resides in our limited knowledge of Cl concentrations in the troposphere. Due to the difficulty of directly observing Cl, estimates of its abundance are usually derived from non-methane hydrocarbons (NMHC) observations. Using this method, Cl concentration

is estimated to be on the order of  $10^4$  atoms  $\text{cm}^{-3}$  ( $0.2\text{-}80 \times 10^4$  atoms  $\text{cm}^{-3}$ ) in the MBL and Antarctic boundary layer (Jobson et al., 1994; Singh et al., 1996; Wingenter et al., 1996; 2005; Boundries and Bottenheim, 2000; Arsene et al., 2007; Read et al., 2007), with highest concentrations over Tropical Pacific during autumn (Singh et al., 1996). However, a recent study suggests that this is an overestimate of tropospheric Cl abundance (Gromov et al., 2018). Another uncertainty in the atmospheric implications of DMS+Cl originates from its sulfur products, which are most likely  $\text{CH}_3\text{SCH}_2$  via the abstraction channel and  $(\text{CH}_3)_2\text{S-Cl}$  adduct via the addition channel (Barnes et al., 2006). The  $\text{CH}_3\text{SCH}_2$  will likely be further oxidized into  $\text{SO}_2$ , similar to the abstraction channel of DMS+OH, while the  $(\text{CH}_3)_2\text{S-Cl}$  adduct could react with  $\text{O}_2$  to produce DMSO. Atkinson et al. (2004) estimated that 50% of DMS+Cl occurs through the abstraction channel and 50% occurs through the addition channel at 298 K and 1 bar pressure, but the abstraction channel could account for more than 95% at low pressure (Butkovskaya et al., 1995). Since DMS+Cl is neither a big sink of DMS nor a big source of DMSO in our study, the yield uncertainties have little influence on the modeled sulfur budgets. However, modeled estimates of DMS+Cl could be too low due to a potential low bias in modeled Cl abundance.

In this study,  $\text{DMS+O}_{3(\text{aq})}$  is the only multiphase DMS oxidation pathway, which accounts for only 2% of DMS oxidation globally, reaching up to 5% over high-latitude oceans (e.g. Southern Ocean) (Fig. 3). In comparison, in a general circulation model Boucher et al. (2003) calculated that  $\text{DMS+O}_{3(\text{aq})}$  accounts for about 6% of DMS oxidation globally and 15-30% over oceans north of  $60^\circ\text{N}$  and in the  $50\text{-}75^\circ\text{S}$  latitude band. The difference between the results from Boucher et al. (2003) and this study could be due to the differences in oxidant abundances such as  $\text{O}_3$ ,  $\text{OH}$ ,  $\text{BrO}$  and  $\text{Cl}$ . Using a 1-D model, von Glasow and Crutzen (2004) calculated that  $\text{DMS+O}_{3(\text{aq})}$  accounts for 4-18% of DMS oxidation in the cloudy MBL, which is similar to 5-10% over the Southern Ocean MBL in our model results. The fraction of DMS oxidized by  $\text{O}_3$  in the gas phase ( $f_{\text{[I]DMS+O}_3\text{[g]}}=0.5\%$ ) is smaller than  $f_{\text{[I]DMS+O}_3\text{[aq]}}$ , consistent with Boucher et al. (2003). Thus, both the gas-phase and multiphase oxidation of DMS by  $\text{O}_3$  represent minor DMS sinks in the global troposphere.

### 3.2 DMSO budget

The modeled global tropospheric DMSO burden is 8 Gg S, which is 3-4 times larger than in Pham et al. (1995) and Cosme et al. (2002) which did not include production of DMSO from DMS+BrO. Modeled surface DMSO mixing ratio is highest over the Southern Ocean ( $\approx 30$  ppt) (Fig. 2b) where the DMS mixing ratio is high and  $\text{BrO}$  is abundant. The high DMSO mixing ratio over Antarctica in our model is due to weak DMSO oxidation by  $\text{OH}$  in both the gas and aqueous phase. DMSO mainly resides in the lower troposphere, with 67% of the tropospheric burden below 2 km.

Globally, we simulate DMS+BrO is the biggest source of DMSO (44%), followed by the addition channel of DMS+OH (41%), DMS+Cl (9%) and  $\text{DMS+O}_{3(\text{aq})}$  (6%). The fraction of DMSO produced from DMS+BrO is highest over the high-latitude ocean where  $\text{OH}$  abundance is low and subtropical oceans where  $\text{BrO}$  abundance is high, while DMS+Cl and

DMSO+O<sub>3(aq)</sub> can account for up to 20% of the DMSO production in coastal regions and mid-latitude MBL, respectively (Fig. 4).

DMSO is removed from the atmosphere via gas-phase oxidation by OH (33%), multiphase oxidation by OH in cloud droplets (37%) and aerosols (3%), and dry (16%) and wet deposition (11%). The lifetime of DMSO is about 11 hours. Multiphase oxidation mainly occurs over regions where clouds are frequent and OH concentrations are high, e.g. low- to mid-latitude oceans (Fig. 5). Cosme et al. (2002) calculated 85% of DMSO is lost via gas-phase oxidation by OH and the rest 15% via deposition in a global 3-D model, but they did not include heterogeneous loss of DMSO. It has been suggested that heterogeneous loss is the predominant loss process of DMSO in the cloudy MBL in box or 1-D models (Zhu et al., 2006; Hoffmann et al., 2016).

### 3.3 MSIA budget

MSIA is an important intermediate during the oxidation of DMSO to produce MSA, and has a simulated tropospheric burden of 2 Gg S. The surface MSIA mixing ratio is higher over Antarctica than over the Southern Ocean (Fig. 2c) due to larger removal of MSIA by O<sub>3(aq)</sub> and OH<sub>(aq)</sub> in clouds over Southern Ocean. 31% of MSIA resides below 2 km altitude. The smaller fraction of MSIA below 2 km compared to DMSO is due to faster oxidation of MSIA by OH<sub>(aq)</sub> and O<sub>3(aq)</sub> in clouds and aerosols (Table 1).

In  $R_{\text{all}}$ , MSIA is produced from both gas-phase (44%) and multiphase (56%) oxidation of DMSO by OH in cloud droplets and aerosols (Fig. 1). Multiphase production of MSIA mainly occurs over low- to mid-latitude oceans where the OH abundance is high and clouds are frequent (Fig. 6).

MSIA is mainly removed in the troposphere via both gas-phase and multiphase oxidation by OH, with a lifetime of 4 hours. Dry (2%) and wet (2%) deposition of MSIA accounts for 4% of MSIA removal in the troposphere. Globally, multiphase oxidation in cloud droplets and aerosols by OH<sub>(aq)</sub> (53%) and O<sub>3(aq)</sub> (24%) is the biggest sink of MSIA, followed by gas-phase oxidation by OH (19%). Multiphase oxidation by OH<sub>(aq)</sub> is more important over low-latitude oceans where OH abundance is high, reaching up to 70% (Fig. 7). Multiphase oxidation by O<sub>3(aq)</sub> is more important over high-latitude ocean where OH abundance is low (Fig. 7). Over continents and Antarctica, MSIA is mostly oxidized by OH in the gas phase.

In comparison, Hoffmann et al. (2016) also found that multiphase oxidation is the main sink of MSIA in the MBL in their box model, with O<sub>3(aq)</sub>, OH<sub>(aq)</sub> and Cl<sup>-</sup> accounting for 42%, 19% and 10% of MSIA removal, respectively. The rest of MSIA (29%) was removed by CH<sub>3</sub>SO<sub>2</sub>(O<sub>2</sub><sup>•</sup>) that was produced as an intermediate during the electron transfer reaction of MSIA with OH<sub>(aq)</sub> and Cl<sup>-</sup> in cloud droplets and aerosols. By considering cloud droplets only, Hoffmann (2016) suggested OH<sub>(aq)</sub> is more important (1.5 times faster) than O<sub>3(aq)</sub> for MSIA oxidation, which is consistent with our results. Since information such

as  $\text{OH}_{(\text{aq})}$  concentrations in aerosols, aerosol water content and cloud liquid water content were not provided in Hoffmann et al. (2016), we do not further compare our MSIA oxidation by  $\text{O}_{3(\text{aq})}$  and  $\text{OH}_{(\text{aq})}$  to Hoffmann et al. (2016). Hoffmann et al. (2016) is the only modeling study that considered multiphase reaction of MSIA with both  $\text{O}_{3(\text{aq})}$  and  $\text{CH}_3\text{SO}_2(\text{O}_2\cdot)$ . Zhu et al. (2006) found  $\text{Cl}_2^-$  to be more important than  $\text{OH}_{(\text{aq})}$  for MSIA oxidation when assuming  $\text{Cl}_2^-$  concentration 6 times higher than that used in Hoffmann et al. (2016). Due to our limited knowledge about  $\text{CH}_3\text{SO}_2(\text{O}_2\cdot)$  and  $\text{Cl}_2^-$  production and concentrations in cloud droplets and aerosols, we do not include the multiphase reactions of MSIA with  $\text{CH}_3\text{SO}_2(\text{O}_2\cdot)$  and  $\text{Cl}_2^-$  in this study.

Gas-phase oxidation of MSIA by OH (18%) has important implications for the MSA budget as  $\text{MSIA}+\text{OH}_{(\text{g})}$  has a low yield for MSA formation ( $\text{SO}_2$  yield of 0.9) (Kukui et al., 2003). Gas-phase oxidation of MSIA by  $\text{O}_3$  is negligible globally (1%). In contrast, Lucas and Prinn (2002) suggest  $\text{MSIA}+\text{O}_{3(\text{g})}$  could compete with  $\text{MSIA}+\text{OH}_{(\text{g})}$  for MSIA removal, but the rate coefficient of  $\text{MSIA}+\text{OH}_{(\text{g})}$  is very small in their 1-D model (about two orders of magnitude smaller than ours).

### 3.4 MSA budget

In  $R_{\text{all}}$ , the global MSA burden is 20 Gg S, which is within the range of 13-40 Gg S reported in previous modeling studies (Pham et al., 1995; Chin et al., 1996; 2000; Cosme et al., 2002; Hezel et al., 2011). The largest MSA burden is from Hezel et al. (2011), in which DMSO was not included, while the smallest MSA burden is from Cosme et al. (2002), in which DMSO was included. Neglecting the DMSO intermediate in the model could result in an overestimate of MSA production as DMSO is also removed via dry and wet deposition. Note that none of these previous studies consider  $\text{DMS}+\text{BrO}$  and  $\text{MSA}+\text{OH}_{(\text{aq})}$  in their models. Surface MSA mixing ratio is highest over the Southern Ocean, but the peak shifts north compared to DMS, DMSO and MSIA (Fig. 2d). This is due to larger production of MSA by  $\text{O}_{3(\text{aq})}$  and  $\text{OH}_{(\text{aq})}$  in clouds (due to higher  $\text{O}_{3(\text{aq})}$  and  $\text{OH}_{(\text{aq})}$  concentrations at lower latitudes) over northern part of Southern Ocean compared to the southern part of Southern Ocean. 57% of MSA resides below 2 km altitude, suggesting that MSA is mainly produced in the MBL.

As shown in Fig. 1, MSA is mainly produced from multiphase oxidation of MSIA by OH (66%) and  $\text{O}_3$  (30%).  $\text{MSIA}+\text{OH}_{(\text{aq})}$  dominates over low-latitude oceans while  $\text{MSIA}+\text{O}_{3(\text{aq})}$  dominates over high-latitude oceans (Fig. 8). MSA formation occurs mainly in clouds (74%), where the liquid water content is high. Our result is consistent with the general concept that gas-phase MSA formation is small compared to multiphase formation (Barnes et al., 2006; von Glasow and Crutzen, 2004; Zhu et al., 2006; Hoffmann et al., 2016). MSA+OH<sub>(aq)</sub> accounts for 12% of MSA removal in  $R_{\text{all}}$ , and the rest of MSA is removed via dry (12%) and wet (76%) deposition. The lifetime of MSA is 2.2 days globally, which is relatively short compared to 5-7 days in previous studies (Pham et al., 1995; Chin et al., 1996; 2000; Cosme et al., 2002; Hezel et al., 2011) without  $\text{MSA}+\text{OH}_{(\text{aq})}$ . Information about the global distribution of MSA concentrations and deposition from these previous modelling studies are needed for comparison. The MSA lifetime is lowest (about 1 day) over tropical oceans where clouds are frequent and OH abundance is high. It increases to 2-6 days over Southern Ocean and subtropical oceans. To the

best of our knowledge, this is the first study to report global MSA lifetime from a global 3-D model that considers MSA+OH<sub>(aq)</sub>. In the sensitivity run without MSA+OH<sub>(aq)</sub> ( $R_{\text{noMSA+OH}_{\text{(aq)}}}$ ), the lifetime of MSA increases to 2.5 days. In the sensitivity run with a higher rate constant of MSA+OH<sub>(aq)</sub> ( $R_{\text{moreMSA+OH}_{\text{(aq)}}}$ ), the lifetime of MSA decreases to 1.7 days.

### 3.5 Uncertainties in rate constants

5 The uncertainties in the rate constants for the reactions added in the model are shown in Table 4. The uncertainty factor ( $f_{298}$ ) used for gas-phase reaction rate constants at 298 K indicates that the reaction rate constant could be greater than or less than the recommended value by a factor of  $f_{298}$ . For all gas-phase reactions added in this study,  $f_{298}$  varies from 1.2 to 1.5.  $f_{298}$  is 1.3 for the DMS+BrO reaction, which adds to the uncertainty in oxidation of DMS by BrO. The global annual mean tropospheric BrO burden varies from 3.6 to 5.7 Gg Br in three recent global modeling studies (Parrella et al., 2012; Schmidt 10 et al., 2016; Chen et al., 2017), but all three of these modeling studies underestimate satellite observations of the tropospheric BrO column from Theys et al. (2010) (e.g. by 44% over Southern Ocean in Chen et al. (2017)). Thus, further investigations are needed in both laboratory determination of the reaction rate constant for DMS+BrO and field observations of the BrO abundance in the troposphere. In addition, we need to better constrain the rate constants for the other two gas-phase reactions 15 DMS+OH (addition pathway) and DMSO+OH ( $f_{298}=1.2$ ). Very few studies have determined the rate constants for the multiphase reactions added in the model (Table 4). The biggest uncertainty resides in the oxidation of MSA by OH<sub>(aq)</sub> and the oxidation of MSIA by O<sub>3(aq)</sub>. The rate constant for the MS<sup>+</sup>+OH<sub>(aq)</sub> reactions differs by a factor of 4.7 in Milne et al. (1989) and Zhu et al. (2003), which results in about 30% difference in global annual mean tropospheric MSA burden. Only 20 one box modeling study (Hoffmann et al., 2016) considered the oxidation of MSIA by O<sub>3(aq)</sub> in clouds and aerosols, using the rate constant measured in Herrmann and Zellner (1997) for the MSIA<sub>(aq)</sub>+O<sub>3(aq)</sub> reaction and Flynt et al. (2001) for the MSI<sup>+</sup>+O<sub>3(aq)</sub> reaction. As MSIA+O<sub>3(aq)</sub> and MSA+OH<sub>(aq)</sub> are important for MSA production and removal, more laboratory studies are needed to constrain the rate constants for these two reactions.

### 3.6 Model-observation comparison

#### 3.6.1 Surface DMS mixing ratio

Monthly mean DMS mixing ratios measured at 4 stations around the globe are used to assess modeled DMS: Crete Island 25 (CI; 35°24'N, 25°60'E) (Kouvarakis and Mihalopoulos, 2002), Amsterdam Island (AI; 37°50'S, 77°30'E) (Castebrunet et al., 2009), Cape Grim (CG; 40°41'S, 144°41'E) (Ayer et al., 1995), and Dumont D'Urville (DU; 66°40'S, 140°1'E) (Castebrunet et al., 2009). The DMS data covers the 1997-1999 period for CI, the 1987-2006 period for AI, the 1989-1992 period for CG, and the 1998-2006 period for DU.

30 Figure 9 shows the comparison between modeled and observed monthly-mean DMS mixing ratio at CI, AI, CG and DU stations. Comparing  $R_{\text{all}}$  with  $R_{\text{std}}$ , we can see that in general the modeled DMS mixing ratios match better with observations

for the three stations in the Southern Hemisphere with the updated DMS chemistry, especially during Southern Hemisphere winter. Between June and August, the modeled DMS mixing ratios calculated from  $R_{\text{std}}$  overestimate observations by a factor of 6, 4 and 27 for AI, CG and DU, respectively. In comparison, during the same period, the modeled DMS mixing ratios calculated from  $R_{\text{all}}$  overestimate observations by a factor of 3 for AI, 50% for CG and a factor of 4 for DU, respectively.

5 The smaller discrepancy between modeled and observed DMS mixing ratio in  $R_{\text{all}}$  is largely due to DMS+BrO, as indicated by comparing  $R_{\text{all}}$  with a model run that includes all reactions except DMS+BrO ( $R_{\text{noDMS+BrO}}$ ). It should be noted that BrO is underestimated in our model compared to satellite observations (underestimated by 44% in terms of annual mean tropospheric BrO column between 30°S and 60°S) (Chen et al., 2017), which might partly explain the remaining overestimate of DMS mixing ratios from  $R_{\text{all}}$  compared to observations.

10

In addition to DMS chemistry shown above, surface seawater DMS concentrations also affect the modeled DMS mixing ratio. The surface seawater DMS concentration was obtained from Kettle et al. (1999) in  $R_{\text{Kettle}}$ , instead of from Lana et al. (2011) in  $R_{\text{all}}$ . The global DMS emission flux from  $R_{\text{Kettle}}$  is 15% lower than that from  $R_{\text{all}}$ . Overall, at CI, CG and DU, the modeled DMS mixing ratios from  $R_{\text{Kettle}}$  are similar to those from  $R_{\text{all}}$  during most of the year. Much lower DMS mixing 15 ratios were calculated from  $R_{\text{Kettle}}$  at CI in June, at CG in January and at DU in December and January. At AI, however, the modeled DMS mixing ratios from  $R_{\text{Kettle}}$  are lower than those from  $R_{\text{all}}$  in general, which agree better with observations except in December and January. In this study, we focus on the chemistry aspects of the sulfur cycle and thus will not present further discussion on the impact of the DMS sea water climatology on atmospheric DMS abundance.

### 3.6.2 Surface MSA/nssSO<sub>4</sub><sup>2-</sup> ratio

20 Figure 10 shows the comparison between modeled and observed annual-mean MSA/nssSO<sub>4</sub><sup>2-</sup> ratio at 23 stations around the globe (Table 5). Data for all stations was obtained from Gondwe et al. (2004), except for CI from Kouvarakis and Mihalopoulos (2002) and AI, PA, KO and DC from Casterbrunet et al. (2009). The global distribution of annual-mean MSA/nssSO<sub>4</sub><sup>2-</sup> obtained from  $R_{\text{all}}$ , overplotted with observations for these 23 stations are shown in Fig. 11. In addition to the 4 model runs described in Sect. 3.6.1 ( $R_{\text{all}}$ ,  $R_{\text{std}}$ ,  $R_{\text{Kettle}}$  and  $R_{\text{noDMS+BrO}}$ ), 5 additional model runs were performed by removing 25 ( $R_{\text{noMSA+OH(aq)}}$ ) or increasing ( $R_{\text{moreMSA+OH(aq)}}$ ) aqueous-phase oxidation of MSA by OH, removing all multiphase chemistry involving DMS, DMSO, MSIA and MSA oxidation ( $R_{\text{noMUL}}$ ), decreasing OH<sub>(aq)</sub> concentrations in cloud droplets and aerosols by two orders of magnitude ( $R_{\text{lowOH(aq)}}$ ), and using a unity yield of DMSO for the addition channel of DMS oxidation by OH ( $R_{\text{add}}$ ) (see Table 3).

30 Figures 10 and 11 show that modeled MSA/nssSO<sub>4</sub><sup>2-</sup> ratios calculated from  $R_{\text{all}}$  can generally reproduce the spatial variability of MSA/nssSO<sub>4</sub><sup>2-</sup> observations, especially the latitudinal trend of increasing ratios towards the south where anthropogenic sources of nssSO<sub>4</sub><sup>2-</sup> are less important. However, modeled MSA/nssSO<sub>4</sub><sup>2-</sup> ratios overestimate observations by a factor of 2 on

average. The normalized mean bias  $N_{MB}$  ( $= \frac{\sum_{i=1}^{23} (M_i - O_i)}{\sum_{i=1}^{23} O_i} \times 100\%$ , where  $M_i$  and  $O_i$  are modeled value and observed value, respectively) for the comparison between modeled and observed MSA/nssSO<sub>4</sub><sup>2-</sup> ratios in  $R_{all}$  is 128%. The large modeled MSA/nssSO<sub>4</sub><sup>2-</sup> over low-latitude oceans (13°N-37°S) is due to lower anthropogenic sources of nssSO<sub>4</sub><sup>2-</sup> and to large multiphase MSA production as a result of high cloud liquid water content and oxidant abundance (OH and O<sub>3</sub>). Over 5 Antarctica (Stations PA, DU, MA, NE, HB, KO and DC) where aqueous-phase oxidation of MSA is small, modeled MSA/nssSO<sub>4</sub><sup>2-</sup> ratios are about twice observations on average. In  $R_{noDMS+BrO}$ , the modeled MSA/nssSO<sub>4</sub><sup>2-</sup> ratios decrease compared to  $R_{all}$ , which is most evident over stations where DMS + BrO is a large source of DMSO and MSA (e.g. Southern 10 Hemisphere ocean and Antarctica) (Fig. 4). Compared to  $R_{all}$ , the modeled MSA/nssSO<sub>4</sub><sup>2-</sup> ratios from  $R_{noDMS+BrO}$  match better with observations, with  $N_{MB}=40\%$ . However, as shown in Sect. 3.6.1, DMS observations were largely overestimated in 15  $R_{noDMS+BrO}$  (Fig. 9). If multiphase chemistry is switched off ( $R_{noMUL}$ ), modeled MSA/nssSO<sub>4</sub><sup>2-</sup> ratios underestimate the observations by 49% on average for all 23 stations. Thus, multiphase sulfur chemistry is important for the model simulation of MSA/nssSO<sub>4</sub><sup>2-</sup> observations. However, the OH<sub>(aq)</sub> concentrations in cloud droplets and aerosols, which range from 10<sup>-14</sup> M to 10<sup>-12</sup> M in modeling studies (Jacob, 1986; Matthijsen et al., 1995; Jacob et al., 1989; Herrmann et al., 2000) and 10<sup>-16</sup> M to 10<sup>-14</sup> M in observations (Arakaki et al., 2013; Kaur and Anastasio, 2017), is a large uncertainty in modeling multiphase 20 sulfur chemistry. The model run reducing OH<sub>(aq)</sub> concentrations by two orders of magnitude ( $R_{lowOH(aq)}$ ) results in 25% decrease in MSA/nssSO<sub>4</sub><sup>2-</sup>, with  $N_{MB}=84\%$ . Due to the small chemical loss of MSA in our model, MSA/nssSO<sub>4</sub><sup>2-</sup> in model run without MSA + OH<sub>(aq)</sub> ( $R_{noMSA+OH(aq)}$ ) is similar to that in  $R_{all}$ . The model run with a larger reaction rate coefficient of MSA + OH<sub>(aq)</sub> ( $R_{moreMSA+OH(aq)}$ ) results in a decrease in modeled MSA/nssSO<sub>4</sub><sup>2-</sup> (24% on average) compared to  $R_{all}$ . This 25 reveals the importance of MSA + OH<sub>(aq)</sub> for MSA/nssSO<sub>4</sub><sup>2-</sup> observations, as suggested by von Glasow and Crutzen (2004), Zhu et al. (2006) and Mungall et al. (2018). The model run with a unity yield of DMSO from the addition channel of DMS oxidation by OH ( $R_{add}$ ) largely overestimates MSA/nssSO<sub>4</sub><sup>2-</sup> observations, with  $N_{MB}=281\%$ .

Modeled MSA/nssSO<sub>4</sub><sup>2-</sup> from  $R_{std}$  without multiphase chemistry and DMS+BrO can generally reproduce the meridional trend of observations, with  $N_{MB}=51\%$ . However,  $R_{std}$  overestimates DMS observations (Fig. 9), suggesting that  $R_{std}$  produces 25 comparable MSA/nssSO<sub>4</sub><sup>2-</sup> values for the wrong reasons.

#### 4 Implications

Once emitted into the atmosphere through air-sea exchange, biogenic DMS undergoes complicated chemical processes to form SO<sub>2</sub> and MSA in the troposphere. SO<sub>2</sub> can then be oxidized to form sulfate aerosol. Sulfate and MSA produced in the gas phase can nucleate new particles under favorable conditions (Kulmala et al., 2000; Chen et al., 2015), while MSA and 30 sulfate produced in the aqueous phase leads to the growth of existing particles (Kreidenweis and Seinfeld, 1988; Kaufman and Tanre, 1994). Global models such as General Circulation Models (GCMs) and Chemical Transport Models (CTMs)

generally consider very simplified gas-phase DMS chemistry, which could result in large biases in SO<sub>2</sub> and MSA prediction. Quantifying the yields of SO<sub>2</sub> and MSA from DMS oxidation is necessary to evaluate the climate impacts of DMS from the ocean ecosystem. Compared to the standard GEOS-Chem model run, the updated sulfur scheme in this study decreases the conversion yield of DMS to SO<sub>2</sub> ( $Y_{\text{DMS} \rightarrow \text{SO}_2}$ ) from 91% to 75% and increases the conversion yield of DMS to MSA (5  $Y_{\text{DMS} \rightarrow \text{MSA}}$ ) from 9% to 15%. The remaining 10% of DMS is lost via wet and dry deposition of DMSO and MSIA. In order to gain insight into the impacts of our updated sulfur scheme on global SO<sub>2</sub>, MSA and sulfate burden, we conducted two sensitivity studies by allowing DMS as the only sulfur source for both the standard model run  $R_{\text{std}}$  ( $R_{\text{std\_onlyDMS}}$ ) and full model run  $R_{\text{all}}$  ( $R_{\text{all\_onlyDMS}}$ ). Compared to  $R_{\text{std\_onlyDMS}}$ , the global DMS, SO<sub>2</sub>, MSA and sulfate burden in  $R_{\text{all\_onlyDMS}}$  decreases by 40%, 17%, 8% and 12%, respectively. The decrease in DMS is mainly due to DMS oxidation by BrO with the updated 10 sulfur scheme. The decrease in SO<sub>2</sub> is due to a lower yield of SO<sub>2</sub> from DMS ( $Y_{\text{DMS} \rightarrow \text{SO}_2}$ ), but is partly compensated by the increase in the DMS oxidation rate. MSA decreases despite an increase in the yield of MSA from DMS ( $Y_{\text{DMS} \rightarrow \text{MSA}}$ ) due to a shorter lifetime in  $R_{\text{all\_onlyDMS}}$  (2.2 days in  $R_{\text{all\_onlyDMS}}$  versus 4.1 days in  $R_{\text{std\_onlyDMS}}$ ) that is caused by the aqueous-phase sink of MSA via MSA + OH<sub>(aq)</sub> and faster deposition of MSA produced in the MBL. The decrease in sulfate is caused by the 15 decrease in SO<sub>2</sub> but is partly compensated by the inclusion of MSA + OH<sub>(aq)</sub> as a sulfate source, which accounts for 4% of global sulfate production. The decrease in sulfate will be smaller if more MSA is oxidized into sulfate instead of being lost via deposition. In sum, climate models with a simplified DMS oxidation scheme (gas-phase oxidation by OH and NO<sub>3</sub> only) 20 may overestimate SO<sub>2</sub>, MSA and sulfate abundances in the pre-industrial environment, potentially leading to underestimates in sulfur aerosol radiative forcing calculations in climate models. Quantifying the impacts of our updated sulfur oxidation scheme on new particle formation is out of the scope of this study and should be addressed in the future.

MSA in Antarctic ice cores has been related to spring sea ice extent (Curran et al., 2003; Abram et al., 2010) as DMS is emitted in regions of sea ice melt. Our results show that, in addition to DMS emission, tropospheric sulfur chemistry is critical for MSA abundance in the troposphere, as also suggested by observations in inland East Antarctica (Legrand et al., 25 2017). Compared to the full model run  $R_{\text{all}}$ , sensitivity studies without DMS+BrO reaction ( $R_{\text{noDMS+BrO}}$ ) and without multiphase oxidation of DMS, DMSO, MSIA and MSA ( $R_{\text{noMUL}}$ ) reduce the global MSA burden by 15% and 75%, respectively. This indicates that reactive halogen and multiphase chemistry are important for the MSA budget in the troposphere, which should be considered when interpreting MSA abundance in ice cores, especially over time periods where the abundance of atmospheric oxidants may have changed.

## 5 Conclusions

30 In this study, we investigate the impacts of reactive halogen and multiphase chemistry on tropospheric DMS chemistry by adding 2 new chemical tracers (DMSO and MSIA) and 12 new reactions for both the gas-phase and multiphase oxidation of DMS, DMSO, MSIA and MSA into a global chemical transport model, GEOS-Chem. With the updated DMS chemistry, the

DMS burden decreases by 40% globally, mostly due to oxidation of DMS by BrO. BrO oxidation accounts for 12% of DMS oxidation globally, which could be underestimated due to underestimates in BrO abundance in the model, but is within the range of 8-16% reported in previous studies. Cl is not important for DMS oxidation due to small Cl abundance, but this reaction should be revisited if modeled Cl budgets are substantially revised in the future. Both gas-phase and multiphase 5 oxidation of DMS by O<sub>3</sub> are not important for the global DMS budget and can be neglected in global models.

Dry and wet deposition accounts for 28% of DMSO removal and 4% of MSIA removal globally. The significant role of deposition as a sink for DMSO suggests that DMSO should be included in sulfur chemistry mechanisms, as exclusion of DMSO as an intermediate may result in an overestimate of MSA production from the oxidation of DMS. MSIA is an 10 important intermediate between DMSO and MSA. MSA is mostly (97% globally) produced through aqueous phase oxidation of MSIA by O<sub>3(aq)</sub> and OH<sub>(aq)</sub> in cloud droplets and aerosols. Dry and wet deposition accounts for 88% of MSA removal globally, multiphase oxidation by OH in cloud droplets and aerosols accounts for the rest. We note that the relative 15 importance of deposition versus oxidation as a sink for MSA will depend on the OH<sub>(aq)</sub> concentration in cloud droplets and aerosols, which is highly uncertain.

15 Modeled DMS mixing ratios agree better (mean square error between model and observation is 44% smaller) with observations with the inclusion of DMS+BrO. The overestimate of MSA/nssSO<sub>4</sub><sup>2-</sup> observations using our updated sulfur oxidation scheme suggests MSA oxidation is underestimated in the model. The uncertainties of reactive halogen abundances such as BrO and Cl and the aqueous phase oxidant concentrations such as OH<sub>(aq)</sub> have limited our ability to model DMS 20 oxidation and MSA formation in the troposphere. Future studies should prioritize the measurements of reactive halogen abundances and OH<sub>(aq)</sub> concentrations in cloud droplets, especially in the marine boundary layer.

### Acknowledgements

We acknowledge Dr. Johan A. Schmidt for the discussions on tropospheric sulfur and halogen cycles, and providing support 25 for the GEOS-Chem halogen chemistry scheme. We acknowledge Dr. Tom Breider for offering help on DMSO simulation scheme. We acknowledge Dr. Paul Hezel for the help on searching for sulfur species observations, and Dr. Giorgos Kouvarakis for providing DMS data on Crete Island. We acknowledge NSF AGS award 1343077 to B.A. for support of this research.

### References

30 Abram, N. J., Thomas, E. R., McConnell, J. R., Mulvaney, R., Bracegirdle, T. J., Sime, L. C., and Aristarain, A. J.: Ice core evidence for a 20th century decline of sea ice in the Bellingshausen Sea, Antarctica, *J. Geophys. Res.*, 115, D23101, doi:10.1029/2010JD014644, 2010.

Alexander, B., Allman, D. J., Amos, H. M., Fairlie, T. D., Dachs, J., Hegg, D. A., and Sletten, R. S.: Isotopic constraints on the formation pathways of sulfate aerosol in the marine boundary layer of the subtropical northeast Atlantic Ocean, *J. Geophys. Res.*, 117, D06304, doi:10.1029/2011JD016773, 2012.

Ammann, M., Cox, R. A., Crowley, J. N., Jenkin, M. E., Mellouki, A., Rossi, M. J., Troe, J., and Wallington, T. J.: 5 Evaluated kinetic and photochemical data for atmospheric chemistry: Volume VI – heterogeneous reactions with liquid substrates, *Atmos. Chem. Phys.*, 13, 8045-8228, doi:10.5194/acp-13-8045-2013, 2013.

Amos, H. M., Jacob, D. J., Holmes, C. D., Fisher, J. A., Wang, Q., Yantosca, R. M., Corbitt, E. S., Galarneau, E., Rutter, A. P., Gustin, M. S., Steffen, A., Schauer, J. J., Graydon, J. A., Louis, V. L. St., Talbot, R. W., Edgerton, E. S., Zhang, Y., and Sunderland, E. M.: Gas-particle partitioning of atmospheric Hg(II) and its effect on global mercury 10 deposition, *Atmos. Chem. Phys.*, 12, 591–603, doi:10.5194/acp-12-591-2012, 2012.

Andreae, M. O.: Ocean-atmosphere interactions in the global biogeochemical sulfur cycle, *Mar. Chem.*, 30, 1–29, doi: 10.1016/0304-4203(90)90059-L, 1990.

Andreae, M. O., Elbert, W., Cai, Y., Andreae, T. W., and Gras, J.: Non-sea-salt sulfate, methanesulfonate, and nitrate 15 aerosol concentrations and size distributions at Cape Grim, Tasmania, *J. Geophys. Res.*, 104, 21 695–21 706, doi: 10.1029/1999JD900283, 1999.

Arakaki, T., Anastasio, C., Kuroki, Y., Nakajima, H., Okada, K., Kotani, Y., Handa, D., Azechi, S., Kimura, T., Tsuhako, A., and Miyagi, Y.: A general scavenging rate constant for reaction of hydroxyl radical with organic carbon in atmospheric waters, *Environ. Sci. Technol.*, 47(15), 8196–8203, doi: 10.1021/es401927b, 2013.

Arsene, C., Bougiatioti, A., Kanakidou, M., Bonsang, B., and Mihalopoulos, N.: Tropospheric OH and Cl levels deduced 20 from non-methane hydrocarbon measurements in a marine site, *Atmos. Chem. Phys.*, 7, 4661-4673, doi:10.5194/acp-7-4661-2007, 2007.

Atkinson, R., Baulch, D. L., Cox, R. A., Crowley, J. N., Hampson, R. F., Hynes, R. G., Jenkin, M. E., Rossi, M. J., and Troe, J.: Evaluated kinetic and photochemical data for atmospheric chemistry: Volume I - gas phase reactions of Ox, HOx, NOx and SOx species, *Atmos. Chem. Phys.*, 4, 1461-1738, doi:10.5194/acp-4-1461-2004, 2004.

Ayers, G. P., Bartley, S. T., Ivey, J. P., and Forgan, B. W.: Dimethylsulfide in marine air at Cape Grim, 41°S, J. 25 Geophys. Res., 100, 21 013–21 021, doi:10.1029/95JD02144, 1995.

Bardouki, H., Barcellos da Rosa, M., Mihalopoulos, N., Palm, W.- U., and Zetzsch, C.: Kinetics and mechanism of the oxidation of dimethylsulfoxide (DMSO) and methanesulfinate (MSI-) by OH radicals in aqueous medium, *Atmos. Environ.*, 36, 4627–4634, doi: 10.1016/S1352-2310(02)00460-0, 2002.

Barnes, I., Hjorth, J., and Mihalopoulos, N.: Dimethyl sulfide and dimethyl sulfoxide and their oxidation in the atmosphere, *Chem. Rev.*, 106 (3), 940-975, doi: 10.1021/cr020529+, 2006.

Becagli, S., Castellano, E., Cerri, O., Curran, M., Frezzotti, M., Marino, F., Morganti, A., Proposito, M., Severi, M., and Traversi, R.: Methanesulphonic acid (MSA) stratigraphy from a Talos Dome ice core as a tool in depicting sea ice 30

changes and southern atmospheric circulation over the previous 140 years, *Atmos. Environ.*, 43, 1051–1058, doi:10.1016/j.atmosenv.2008.11.015, 2009.

Berglen, T. F., Berntsen, T. K., Isaksen, I. S. A., and Sundet, J. K.: A global model of the coupled sulfur/oxidant chemistry in the troposphere: The sulfur cycle, *J. Geophys. Res.*, 109, D19310, doi:10.1029/2003JD003948, 2004.

5 Bey, I., Jacob, D. J., Yantosca, R. M., Logan, J. A., Field, B. D., Fiore, A. M., Li, Q., Liu, H. Y., Mickley, L. J., and Schultz, M. G.: Global modeling of tropospheric chemistry with assimilated meteorology: Model description and evaluation, *J. Geophys. Res.*, 106, 23 073–23 095, doi: 10.1029/2001JD000807, 2001.

Boucher, O., Moulin, C., Belviso, S., Aumont, O., Bopp, L., Cosme, E., von Kuhlmann, R., Lawrence, M. G., Pham, M., Reddy, M. S., Sciare, J., and Venkataraman, C.: DMS atmospheric concentrations and sulphate aerosol indirect  
10 radiative forcing: a sensitivity study to the DMS source representation and oxidation, *Atmos. Chem. Phys.*, 3, 49–65, doi: 10.5194/acp-3-49-2003, 2003.

Boudries, H., and Bottenheim, J. W.: Cl and Br atom concentrations during a surface boundary layer ozone depletion event in the Canadian High Arctic, *Geophys. Res. Lett.*, 27, 517–520, doi: 10.1029/1999GL011025, 2000.

Bräuer, P., Tilgner, A., Wolke, R., and Herrmann, H.: Mechanism development and modelling of tropospheric  
15 multiphase halogen chemistry: The CAPRAM Halogen Module 2.0 (HM2), *J. Atmos. Chem.*, 70, 19–52, doi: 10.1007/s10874-013-9249-6.

Breider, T. J., Chipperfield, M. P., Richards, N. A. D., Carslaw, K. S., Mann, G. W., and Spracklen, D. V.: Impact of BrO on dimethylsulfide in the remote marine boundary layer, *Geophys. Res. Lett.*, 37, L02807, doi:10.1029/2009GL040868, 2010.

20 Burkholder, J. B., Sander, S. P., Abbatt, J., Barker, J. R., Huie, R. E., Kolb, C. E., Kurylo, M. J., Orkin, V. L., Wilmouth, D. M., and Wine, P. H.: Chemical Kinetics and Photochemical Data for Use in Atmospheric Studies, Evaluation No. 18, JPL Publication 15-10, Jet Propulsion Laboratory, Pasadena, <http://jpodataeval.jpl.nasa.gov>, 2015.

Butkovskaya, N. I., and Le Bras, G.: Mechanism of the NO<sub>3</sub>+DMS reaction by discharge flow mass spectrometry, *J. Phys. Chem.*, 98(10), 2582–2591, doi: 10.1021/j100061a014, 1994.

25 Campolongo, F., Saltelli, A., Jensen, N. R., Wilson, J., and Hjorth, J.: The role of multiphase chemistry in the oxidation of dimethylsulfide (DMS) - A latitude dependent analysis, *J. Atmos. Chem.*, 32(3), 327-356, doi: 10.1023/A:1006154618511, 1999.

Carslaw, K. S., Lee, L. A., Reddington, C. L., Pringle, K. J., Rap, A., Forster, P. M., Mann, G. W., Spracklen, D. V., Woodhouse, M. T., Regayre, L. A., and Pierce, J. R.: Large contribution of natural aerosols to uncertainty in indirect  
30 forcing, *Nature*, 503, 67–71, doi:10.1038/nature12674, 2013.

Castebrunet, H., Martinerie, P., Genthon, C., and Cosme, E.: A three-dimensional model study of methanesulphonic acid to non sea salt sulphate ratio at mid and high-southern latitudes, *Atmos. Chem. Phys.*, 9, 9449–9469, doi:10.5194/acp-9-9449-2009, 2009.

Charlson, R. J., Lovelock, J. E., Andreae, M. O., and Warren, S. G.: Oceanic phytoplankton, atmospheric sulphur, cloud albedo and climate, *Nature*, 326 (6114), 655–661, doi: 10.1038/326655a0, 1987.

Chatfield, R. B. and Crutzen, P. J.: Are there interactions of iodine and sulfur species in marine air photochemistry?, *J. Geophys. Res.*, 95(D13), 22319–22341, doi:10.1029/JD095iD13p22319, 1990.

5 Chen, H., Ezell, M. J., Arquero, K. D., Varner, M. E., Dawson, M. L., Gerber, R. B., and Finlayson-Pitts, B. J.: New particle formation and growth from methanesulfonic acid, trimethylamine and water, *Phys. Chem. Chem. Phys.*, 17, 13699-13709, doi:10.1039/c5cp00838g, 2015.

Chen, Q., Geng, L., Schmidt, J. A., Xie, Z., Kang, H., Dachs, J., Cole-Dai, J., Schauer, A. J., Camp, M. G., and Alexander, B.: Isotopic constraints on the role of hypohalous acids in sulfate aerosol formation in the remote marine 10 boundary layer, *Atmos. Chem. Phys.*, 16, 11433-11450, doi: 10.5194/acp-16-11433-2016, 2016.

Chen, Q., Schmidt, J. A., Shah, V., Jaeglé, L., Sherwen, T., and Alexander, B.: Sulfate production by reactive bromine: Implications for the global sulfur and reactive bromine budgets, *Geophys. Res. Lett.*, 44, 7069–7078, doi:10.1002/2017GL073812, 2017.

15 Chin, M., Jacob, D. J., Gardner, G. M., Foreman-Fowler, M. S., Spiro, P. A., and Savoie, D. L.: A global three-dimensional model of tropospheric sulfate, *J. Geophys. Res.*, 101(D13), 18667–18690, doi:10.1029/96JD01221, 1996.

Chin, M., Jacob, D. J., Gardner, G. M., Foreman-Fowler, M. S., Spiro, P. A., and Savoie, D. L.: A global three-dimensional model of tropospheric sulfate, *J. Geophys. Res.*, 101(D13), 18667–18690, doi:10.1029/96JD01221, 1996.

20 Cosme, E., Genthon, C., Martinerie, P., Boucher, O., and Pham, M.: The sulfer cycle at high-southern latitudes in the LMDZT General Circulation Model, *J. Geophys. Res.*, 107(D23), 4690, doi:10.1029/2002JD002149, 2002.

Curran, M. A. J., van Ommen, T. D., Morgan, V. I., Phillips, K. L., and Palmer, A. S.: Ice core evidence for Antarctic sea ice decline since the 1950s, *Science*, 302(5648), 1203–1206, doi:10.1126/science.1087888, 2003.

Du, L., Xu, Y., Ge, M., Jia, L., Yao, L. and Wang, W.: Rate constant of the gas phase reaction of dimethyl sulfide 25 (CH<sub>3</sub>SCH<sub>3</sub>) with ozone, *Chem. Phys. Lett.*, 436(1), 36-40, doi:10.1016/j.cplett.2007.01.025, 2007.

Faloona, I.: Sulfur processing in the marine atmospheric boundary layer: A review and critical assessment of modeling uncertainties, *Atmos. Environ.*, 43, 2841–2854, doi:10.1016/ j.atmosenv.2009.02.043, 2009.

Fisher, J. A., Murray, L. T., Jones, D. B. A., and Deutscher, N. M.: Improved method for linear carbon monoxide simulation and source attribution in atmospheric chemistry models illustrated using GEOS-Chem v9, *Geosci. Model 30 Dev.*, 10, 4129-4144, doi:10.5194/gmd-10-4129-2017, 2017.

Flyunt, R., Makogon, O., Schuchmann, M. N., Asmus, K. D., and von Sonntag, C.: OH-Radical-induced oxidation of methanesulfinic acid. The reactions of the methanesulfonyl radical in the absence and presence of dioxygen, *J. Chem. Soc. Perkin Trans. 2*, 5, 787-792, doi: 10.1039/B009631H, 2001.

Gershenzon, M., Davidovits, P., Jayne, J. T., Kolb, C. E., and Worsnop, D. R.: Simultaneous uptake of DMS and ozone on water, *J. Phys. Chem. A*, 105, 7031–7036, doi:10.1021/jp010696y, 2001.

Gondwe, M., Krol, M., Gieskes, W., Klaassen, W., and de Baar, H.: The contribution of ocean-leaving DMS to the global atmospheric burdens of DMS, MSA, SO<sub>2</sub>, and NSS SO<sub>4</sub><sup>2-</sup>, *Global Biogeochem. Cycles*, 17, 1056, 5 doi:10.1029/2002GB001937, 2003.

Gondwe, M., Krol, M., Klassen, W., Gieskes, W., and De Baar, H.: Comparison of modeled versus measured MSA:nss SO<sub>4</sub><sup>2-</sup> ratios: A global analysis, *Global Biogeochem. Cy.*, 18, GB2006, doi:10.1029/2003GB002144, 2004.

Gromov, S., Brenninkmeijer, C. A. M., and Jöckel, P.: A very limited role of tropospheric chlorine as a sink of the greenhouse gas methane, *Atmos. Chem. Phys.*, 18, 9831–9843, doi:10.5194/acp-18-9831-2018, 2018.

10 Herrmann, H. and Zellner, R.: Removal and interconversions of oxidants in the atmospheric aqueous phase, Part 2 (RINOXA 2), Universität Essen, 1997.

Herrmann, H., Ervens, B., Jacobi, H.-W., Wolke, R., Nowacki, P., and Zellner, R.: CAPRAM2.3: A Chemical Aqueous Phase Radical Mechanism for Tropospheric Chemistry, *J. Atmos. Chem.*, 36, 231–284, doi:10.1023/A:1006318622743, 2000.

15 Hezel, P. J., Alexander, B., Bitz, C. M., Steig, E. J., Holmes, C. D., Yang, X., and Sciare, J.: Modeled methanesulfonic acid (MSA) deposition in Antarctica and its relationship to sea ice, *J. Geophys. Res.*, 116, D23214, doi:10.1029/2011JD016383, 2011.

Hoffmann, E. H., Tilgner, A., Schrödner, R., Bräuer, P., Wolke, R., and Herrmann, H.: An advanced modeling study on the impacts and atmospheric implications of multiphase dimethyl sulfide chemistry, *P. Natl. Acad. Sci. USA*, 113, 20 11776–11781, doi: 10.1073/pnas.1606320113, 2016.

Hossaini, R., Chipperfield, M. P., Saiz-Lopez, A., Fernandez, R., Monks, S., Feng, W., Brauer, P., and von Glasow, R.: A global model of tropospheric chlorine chemistry: Organic versus inorganic sources and impact on methane oxidation, *J. Geophys. Res. Atmos.*, 121, 14,271–14,297, doi:10.1002/2016JD025756, 2016.

Jacob, D. J.: Chemistry of OH in remote clouds and its role in the production of formic acid and peroxymonosulfate, *J. Geophys. Res.*, 91(D9), 9807–9826, doi:10.1029/JD091iD09p09807, 1986.

Jacob, D. J., Gottlieb, E. W., and Prather, M. J.: Chemistry of a polluted cloudy boundary layer, *J. Geophys. Res. Atmos.*, 94(D10), 12975–13002, doi: 10.1029/JD094iD10p12975, 1989.

Jacob, D. J., Field, B. D., Li, Q., Blake, D. R., de Gouw, J., Warneke, C., Hansel, A., Wisthaler, A., Singh, H. B., and Guenther, A.: Global budget of methanol: Constraints from atmospheric observations, *J. Geophys. Res.*, 110, 30 D08303, doi:10.1029/2004JD005172, 2005.

Jaeglé, L., Quinn, P. K., Bates, T. S., Alexander, B., and Lin, J.-T.: Global distribution of sea salt aerosols: new constraints from in situ and remote sensing observations, *Atmos. Chem. Phys.*, 11, 3137–3157, doi:10.5194/acp-11-3137-2011, 2011.

Jobson, B. T., Niki, H., Yokouchi, Y., Bottenheim, J., Hopper, F., and Leaitch, R.: Measurements of C2-C6 hydrocarbons during the Polar Sunrise 1992 Experiment: Evidence for Cl atom and Br atom chemistry, *J. Geophys. Res.*, 99, 25 355–25 368, doi: 10.1029/94JD01243, 1994.

Kaufman, Y. and Tanre, D.: Effect of variations in super-saturation on the formation of cloud condensation nuclei, *Nature*, 369, 45–48, doi:10.1038/369045a0, 1994.

Kaur, R. and Anastasio, C.: Light absorption and the photoformation of hydroxyl radical and singlet oxygen in fog waters, *Atmos. Environ.*, 164, 387-397, doi: 10.1016/j.atmosenv.2017.06.006, 2017.

Kettle, A., Andreae, M., Amouroux, D., Andreae, T., Bates, T., Berresheim, H., Bingemer, H., Boniforti, R., Curran, M., DiTullio, G., Helas, G., Jones, G., Keller, M., Kiene, R., Leck, C., Levasseur, M., Malin, G., Maspero, M., Matrai, P., McTaggart, A., Mihalopoulos, N., Nguyen, B., Novo, A., Putaud, J., Rapsomanikis, S., Roberts, G., Schebeske, G., Sharma, S., Simo, R., Staubes, R., Turner, S., and Uher, G.: A global database of sea surface dimethylsulfide (DMS) measurements and a procedure to predict sea surface DMS as a function of latitude, longitude, and month, *Global Biogeochem. Cy.*, 13, 399–444, doi: 10.1029/1999GB900004, 1999.

Khan, M. A. H., Gillespie, S. M. P., Razis, B., Xiao, P., DaviesColeman, M. T., Percival, C. J., Derwent, R. G., Dyke, J. M., Ghosh, M. V., Lee, E. P. F., and Shallcross, D. E.: A modelling study of the atmospheric chemistry of DMS using the global model, STOCHEM-CRI, *Atmos. Environ.*, 127, 69–79, doi: 10.1016/j.atmosenv.2015.12.028, 2016.

Kloster, S., Feichter, J., Maier-Reimer, E., Six, K. D., Stier, P., and Wetzel, P.: DMS cycle in the marine ocean-atmosphere system – a global model study, *Biogeosciences*, 3, 29–51, doi:10.5194/bg-3-29-2006, 2006.

Kouvarakis, G. and Mihalopoulos, N.: Seasonal variation of dimethylsulfide in the gas phase and of methanesulfonate and non-sea-salt sulfate in the aerosols phase in the eastern Mediterranean atmosphere, *Atmos. Environ.*, 36, 929–938, doi:10.1016/S1352-2310(01)00511-8, 2002.

Kreidenweis, S. M. and Seinfeld, J. H.: Nucleation of sulfuric acid-water and methanesulfonic acid-water solution particles: implications for the atmospheric chemistry of organosulfur species, *Atmos. Environ.*, 22(2), 283-296, doi: 10.1016/0004-6981(88)90034-0, 1988.

Kukui, A., Borissenko, D., Laverdet, G., and Bras, G. L.: Gas phase reactions of OH radicals with dimethyl sulfoxide and methane sulfonic acid using turbulent flow reactor and chemical ionization mass spectrometry, *J. Phys. Chem. A*, 107, 5732–5742, doi:10.1021/jp0276911, 2003.

Kulmala, M., Pirjola, L., and Mäkelä, J. M.: Stable sulphate clusters as a source of new atmospheric particles, *Nature*, 404, 66–69, doi:10.1038/35003550, 2000.

Lana, A., Bell, T. G., Simó, R., Vallina, S. M., Ballabriga-Poy, J., Kettle, A. J., Dachs, J., Bopp, L., Saltzman, E. S., Steffels, J., Johnson, J. E., and Liss, P. S.: An updated climatology of surface dimethylsulfide concentrations and emission fluxes in the global ocean, *Global Biogeochem. Cy.*, 25, GB1004, doi:10.1029/2010GB003850, 2011.

Lee, Y.-N. and Zhou, X.: Aqueous reaction kinetics of ozone and dimethylsulfide and its atmospheric implications, *J. Geophys. Res.*, 99(D2), 3597–3605, doi:10.1029/93JD02919, 1994.

Legrand, M., Preunkert, S., Weller, R., Zipf, L., Elsässer, C., Merchel, S., Rugel, G., and Wagenbach, D.: Year-round record of bulk and size-segregated aerosol composition in central Antarctica (Concordia site) – Part 2: Biogenic sulfur (sulfate and methanesulfonate) aerosol, *Atmos. Chem. Phys.*, 17, 14055–14073, doi:10.5194/acp-17-14055-2017, 2017.

5 Liu, Q.: Kinetics of aqueous phase reactions related to ozone depletion in the arctic troposphere: bromine chloride hydrolysis, bromide ion with ozone, and sulfur(IV) with bromine and hypobromous acid, Ph.D. thesis, Department of Chemistry, Purdue University, USA, 253 pp., 2000.

Liu, Q. and Margerum, D. W.: Equilibrium and kinetics of bromine chloride hydrolysis, *Environ. Sci. Tech.*, 35, 1127–1133, doi: 10.1021/es001380r, 2001.

10 Lucas, D. D. and Prinn, R. G.: Mechanistic studies of dimethylsulfide oxidation products using an observationally constrained model, *J. Geophys. Res.*, 107, doi: 10.1029/2001JD000843, 2002.

Martin, L. R. and Good, T. W.: Catalyzed oxidation of sulfur dioxide in solution: The iron-manganese synergism, *Atmos. Environ.*, 25A, 2395–2399, doi:10.1016/096016869190113L, 1991.

15 Matthijsen, J., Buultjes, P. J. H., and Sedlak, D. L.: Cloud model experiments of the effect of iron and copper on tropospheric ozone under marine and continental conditions, *Met. Atmos. Phys.*, 57(1–4), 43–60, doi: 10.1007/BF01044153, 1995.

Milne, P. J., Zika, R. G., and Saltzman, E. S.: Rate of reaction of dimethyl sulfoxide, and dimethyl sulfone with hydroxyl radical in aqueous solution, American Chemical Society, ACS Symposium Series, American Chemical Society, Washington, DC, pp. 518–528 (Chapter 33), 1989.

20 Mungall, E., Wong, J. P. S., and Abbatt, J. P. D.: Heterogeneous oxidation of particulate methane sulfonic acid by the hydroxyl radical: kinetics and atmospheric implications, *ACS Earth Space Chem.*, 2(1), 48–55, doi: 10.1021/acsearthspacechem.7b00114, 2018.

Park, R. J., Jacob, D. J., Field, B. D., Yantosca, R. M., and Chin, M.: Natural and transboundary pollution influences on sulfate-nitrate- ammonium aerosols in the United States: Implications for policy, *J. Geophys. Res.*, 109, D15204, doi:10.1029/2003JD004473, 2004.

25 Parrella, J. P., Jacob, D. J., Liang, Q., Zhang, Y., Mickley, L. J., Miller, B., Evans, M. J., Yang, X., Pyle, J. A., Theys, N., and Van Roozendael, M.: Tropospheric bromine chemistry: implications for present and pre-industrial ozone and mercury, *Atmos. Chem. Phys.*, 12, 6723–6740, doi:10.5194/acp-12-6723-2012, 2012.

Pham, M., Müller, J., Brasseur, G. P., Granier, C., and Mégie, G.: A three-dimensional study of the tropospheric sulfur 30 cycle, *J. Geophys. Res.*, 100, 26,061– 26,092, doi: 10.1029/95JD02095, 1995.

Pye, H. O. T., Liao, H., Wu, S., Mickley, L. J., Jacob, D. J., Henze, D. K., and Seinfeld, J. H.: Effect of changes in climate and emissions on future sulfate-nitrate-ammonium aerosol levels in the United States, *J. Geophys. Res.*, 114, D01205, doi:10.1029/2008JD010701, 2009.

Ravishankara, A. R., Rudich, Y., Talukdar, R., and Barone, S. B.: Oxidation of atmospheric reduced sulphur compounds: perspective from laboratory studies, *Phil. Trans. R. Soc. Lond. B.*, 352, 171–182, doi:10.1098/rstb.1997.0012, 1997.

Read, K. A., Lewis, A. C., Salmon, R. A., Jones, A. E., and Bauguitte, S.: OH and halogen influence on the variability of nonmethane hydrocarbons in the Antarctic Boundary Layer, *Tellus B.*, 59, 22–38, doi:10.1111/j.1600-0889.2006.00227.x, 2007.

Read, K. A., Lewis, A. C., Bauguitte, S., Rankin, A. M., Salmon, R. A., Wolff, E. W., Saiz-Lopez, A., Bloss, W. J., Heard, D. E., Lee, J. D., and Plane, J. M. C.: DMS and MSA measurements in the Antarctic Boundary Layer: impact of BrO on MSA production, *Atmos. Chem. Phys.*, 8, 2985–2997, doi:10.5194/acp-8-2985-2008, 2008.

Saltzman, E. S., King, D. B., Holmen, K., and Leck, C.: Experimental determination of the diffusion coefficient of dimethylsulfide in water, *J. Geophys. Res.-Oceans*, 98, 16481–16486, doi:10.1029/93JC01858, 1993.

Savoie, D. L., Arimoto, R., Keene, W. C., Prospero, J. M., Duce, R. A., and Galloway, J. N.: Marine biogenic and anthropogenic contributions to non-sea-salt sulfate in the marine boundary layer over the North Atlantic Ocean, *J. Geophys. Res.*, 107, AAC3-1-AAC3-21, doi:10.1029/2001JD000970, 2002.

Schmidt, J. A., Jacob, D. J., Horowitz, H. M., Hu, L., Sherwen, T., Evans, M. J., Liang, Q., Suleiman, R. M., Oram, D. E., Le Breton, M., Percival, C. J., Wang, S., Dix, B., and Volkamer, R.: Modeling the observed tropospheric BrO background: Importance of multiphase chemistry and implications for ozone, OH, and mercury, *J. Geophys. Res.-Atmos.*, 121(11), 155–157, doi:10.1002/2015JD024229, 2016.

Schweitzer, F., Magi, L., Mirabel, P., and George, C.: Uptake rate measurements of methanesulfonic acid and glyoxal by aqueous droplets, *J. Phys. Chem. A*, 102, 593–600, doi: 10.1021/jp972451k, 1998.

Sehested, K. and Holeman, J.: A pulse radiolysis study of the OH radical induced autoxidation of methanesulfinic acid, *Radiat. Phys. Chem.*, 47(3), 357–360, doi:10.1016/0969-806X(95)00115-E, 1996.

Sherwen, T., Schmidt, J. A., Evans, M. J., Carpenter, L. J., Großmann, K., Eastham, S. D., Jacob, D. J., Dix, B., Koenig, T. K., Sinreich, R., Ortega, I., Volkamer, R., Saiz-Lopez, A., Prados-Roman, C., Mahajan, A. S., and Ordóñez, C.: Global impacts of tropospheric halogens (Cl, Br, I) on oxidants and composition in GEOS-Chem, *Atmos. Chem. Phys.*, 16, 12239–12271, doi:10.5194/acp-16-12239-2016, 2016.

Simpson, W. R., Brown, S. S., Saiz-Lopez, A., Thornton, J. A., and von Glasow, R.: Tropospheric Halogen Chemistry: Sources, Cycling, and Impacts, *Chem. Rev.*, 115, 4035–4062, doi:10.1021/cr5006638, 2015.

Singh, H. B., Gregory, G. L., Anderson, B., Browell, E., Sachse, G. W., Davis, D. D., Crawford, J., Bradshaw, J. D., Talbot, R., Blake, D. R., Thornton, D., Newell, R., and Merill, J.: Low ozone in the marine boundary layer of the tropical Pacific ocean: Photochemical loss, chlorine atoms, and entrainment, *J. Geophys. Res.*, 101, 1907–1917, doi: 10.1029/95JD01028, 1996.

Spracklen, D. V., Pringle, K. J., Carslaw, K. S., Chipperfield, M. P., and Mann, G. W.: A global off-line model of size-resolved aerosol microphysics: I. Model development and prediction of aerosol properties, *Atmos. Chem. Phys.*, 5, 2227–2252, doi:10.5194/acp-5-2227-2005, 2005.

Stefels, J., Steinke, M., Turner, S., Mailin, G., and Belviso, S.: Environmental constraints on the production and removal of the climatically active gas dimethylsulphide (DMS) and implications for ecosystem modelling, *Biogeochemistry*, 83, 245–275, doi: 10.1007/s10533-007-9091-5, 2007.

Theys, N., Van Roozendael, M., Hendrick, F., Yang, X., De Smedt, I., Richter, A., Begoin, M., Errera, Q., Johnston, P. V., Kreher, K., and De Mazière, M.: Global observations of tropospheric BrO columns using GOME-2 satellite data, *Atmos. Chem. Phys.*, 11, 1791-1811, doi:10.5194/acp-11-1791-2011, 2011.

Thomas, M. A., Suntharalingam, P., Pozzoli, L., Rast, S., Devasthale, A., Kloster, S., Feichter, J., and Lenton, T. M.: Quantification of DMS aerosol-cloud-climate interactions using the ECHAM5-HAMMOZ model in a current climate scenario, *Atmos. Chem. Phys.*, 10, 7425-7438, doi:10.5194/acp-10-7425-2010, 2010.

10 Troy, R. C. and Margerum, D. W.: Non-metal redox kinetics: Hypobromite and hypobromous acid reactions with iodide and with sulfite and the hydrolysis of bromosulfate, *Inorg. Chem.*, 30, 3538–3543, doi:10.1021/ic00018a028, 1991.

von Glasow, R. and Crutzen, P. J.: Model study of multiphase DMS oxidation with a focus on halogens, *Atmos. Chem. Phys.*, 4, 589-608, doi:10.5194/acp-4-589-2004, 2004.

von Glasow, R., von Kuhlmann, R., Lawrence, M. G., Platt, U., and Crutzen, P. J.: Impact of reactive bromine chemistry in the troposphere, *Atmos. Chem. Phys.*, 4, 2481-2497, doi:10.5194/acp-4-2481-2004, 2004.

15 Wang, Y., Jacob, D. J., and Logan, J. A.: Global simulation of tropospheric O<sub>3</sub>-NO<sub>x</sub> -hydrocarbon chemistry: 1. Model formulation, *J. Geophys. Res.*, 103(D9), 10713–10725, doi:10.1029/98JD00158, 1998.

Wingenter, O. W., Kubo, M. K., Blake, N. J., Smith, T. W., Blake, D. R., and Rowland, F. S.: Hydrocarbon and halocarbon measurements as photochemical and dynamical indicators of atmospheric hydroxyl, atomic chlorine, and 20 vertical mixing obtained during Lagrangian flights, *J. Geophys. Res.*, 101, 4331–4340, doi:10.1029/95JD02457, 1996.

Wingenter, O. W., Sive, B. C., Blake, N. J., Blake, D. R., and Rowland, F. S.: Atomic chlorine concentrations derived from ethane and hydroxyl measurements over the equatorial Pacific Ocean: Implication for dimethyl sulphide and bromine monoxide, *J. Geophys. Res.*, 110, D20308, doi:10.1029/2005JD005875, 2005.

25 Zhang, L., Gong, S.-L., Padro, J., and Barrie, L.: A Size-segregated Particle Dry Deposition Scheme for an Atmospheric Aerosol Module, *Atmos. Environ.*, 35(3), 549–560, doi:10.1016/S1352-2310(00)00326-5, 2001.

Zhu, L., Nicovich, J. M., and Wine, P. H.: Temperature-dependent kinetics studies of aqueous phase reactions of hydroxyl radicals with dimethylsulfoxide, dimethylsulfone, and methanesulfonate, *Aquat. Sci.*, 65, 425– 435, doi:10.1007/s00027-003-0673-6, 2003.

30 Zhu, L., Nicovich, J. M., and Wine, P. H.: Kinetics studies of aqueous phase reactions of Cl atoms and Cl<sub>2</sub>- radicals with organic sulfur compounds of atmospheric interest, *J. Phys. Chem. A*, 109, 3903– 3911, doi: 10.1021/jp044306u, 2005.

Zhu, L., Nenes, A., Wine, P. H., and Nicovich, J. M.: Effects of aqueous organosulfur chemistry on particulate methanesulfonate to non-sea salt sulfate ratios in the marine atmosphere, *J. Geophys. Res.*, 111, D05316, doi:10.1029/2005JD006326, 2006.

5

10

15

20

25

30

24

## Figures

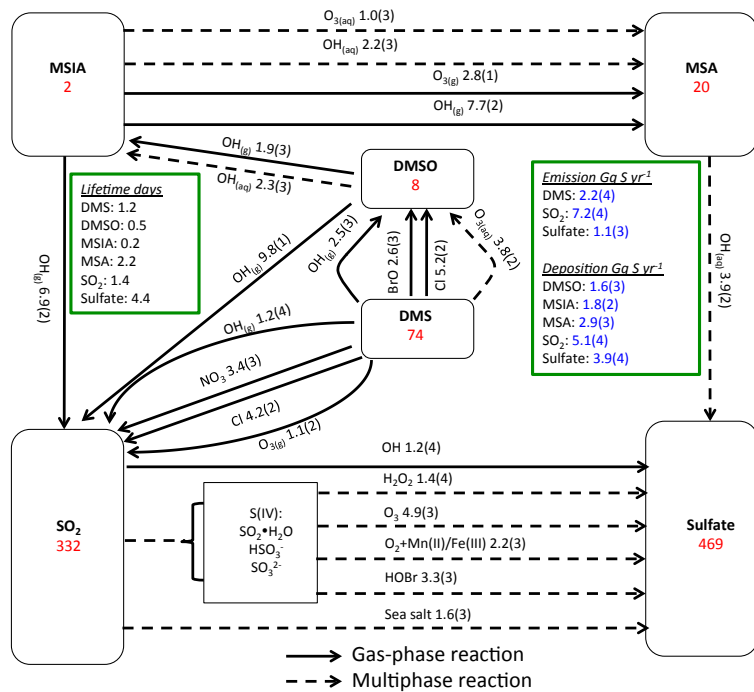


Figure 1: Global sulfur budgets for  $R_{\text{all}}$ . Inventories (inside the boxes) are in units of Gg S. Solid arrows represent gas-phase reactions while dashed arrows represent aqueous-phase reactions. Production and loss rates above arrows are in the unit Gg S yr<sup>-1</sup>. Read 1.9(3) as  $1.9 \times 10^3$  Gg S yr<sup>-1</sup>.

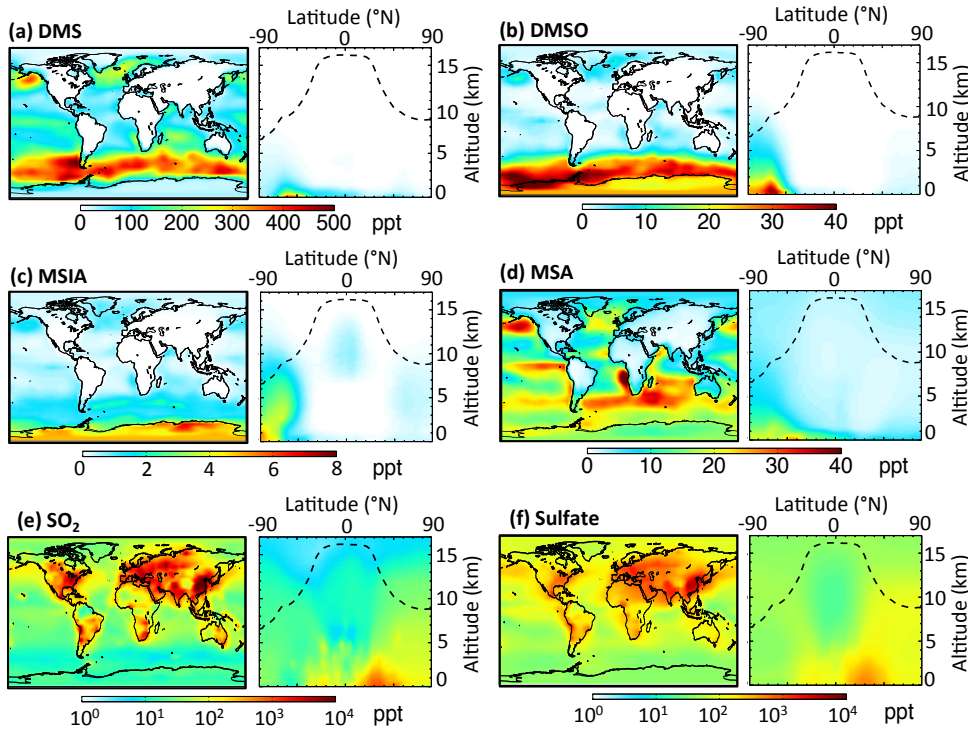


Figure 2: Horizontal distribution of annual-mean surface mixing ratios (ppt) and vertical distribution of mixing ratios for (a) DMS, (b) DMSO, (c) MSIA, (d) MSA, (e) SO<sub>2</sub> and (f) sulfate. The dashed line indicates the climatological tropopause height.

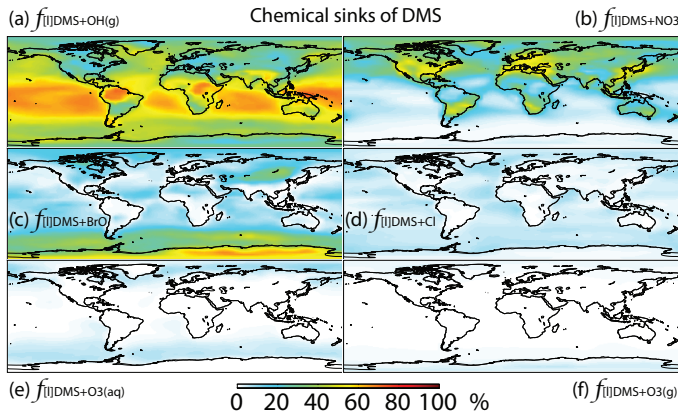


Figure 3: Global tropospheric distribution of annual-mean percentage of DMS oxidized in the troposphere via (a) DMS+OH<sub>(g)</sub> ( $f_{II|DMS+OH(g)}$ ), (b) DMS+NO<sub>3</sub> ( $f_{II|DMS+NO_3}$ ), (c) DMS+BrO ( $f_{II|DMS+BrO}$ ), (d) DMS+Cl ( $f_{II|DMS+Cl}$ ), (e) DMS+O<sub>3(aq)</sub> ( $f_{II|DMS+O3(aq)}$ ) and (f) DMS+O<sub>3(g)</sub> ( $f_{II|DMS+O3(g)}$ ).

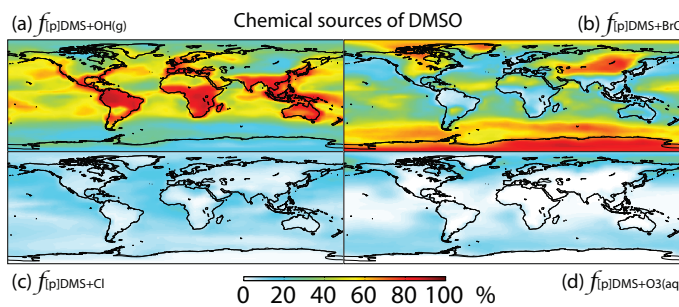


Figure 4: Global tropospheric distribution of annual-mean percentage of DMSO produced via (a) DMS+OH<sub>(g)</sub> ( $f_{[p]DMS+OH(g)}$ ), (b) DMS+BrO ( $f_{[p]DMS+BrO}$ ), (c) DMS+Cl ( $f_{[p]DMS+Cl}$ ) and (d) DMS+O<sub>3(aq)</sub> ( $f_{[p]DMS+O3(aq)}$ ).

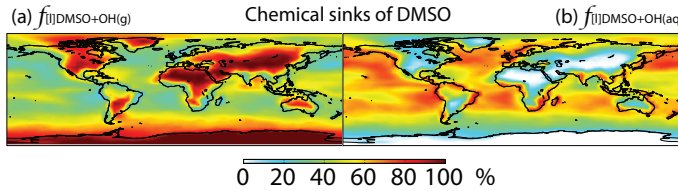


Figure 5: Global tropospheric distribution of annual-mean percentage of DMSO oxidized via (a)  $\text{DMSO}+\text{OH}_{\text{(g)}}$  ( $f_{\text{I}}[\text{DMSO}+\text{OH}_{\text{(g)}}$ ) and (b)  $\text{DMSO}+\text{OH}_{\text{(aq)}}$  ( $f_{\text{I}}[\text{DMSO}+\text{OH}_{\text{(aq)}}$ )).

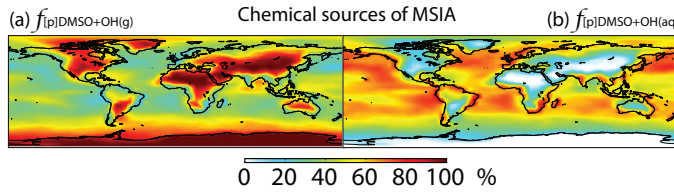


Figure 6: Global tropospheric distribution of annual-mean percentage of MSIA produced in the troposphere via (a)  $\text{DMSO}+\text{OH}_{\text{(g)}}$  ( $f_{\text{p}}[\text{DMSO}+\text{OH}_{\text{(g)}}$ ) and (b)  $\text{DMSO}+\text{OH}_{\text{(aq)}}$  ( $f_{\text{p}}[\text{DMSO}+\text{OH}_{\text{(aq)}}$ )).

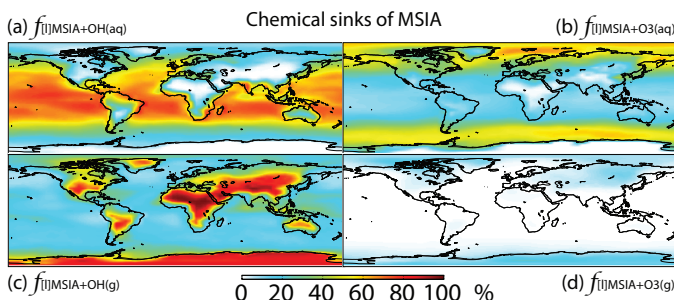


Figure 7: Global tropospheric distribution of annual-mean percentage of MSIA oxidized in the troposphere via (a)  $\text{MSIA}+\text{OH}_{\text{(aq)}}$  ( $f_{\text{I}}[\text{MSIA}+\text{OH}_{\text{(aq)}}$ ), (b)  $\text{MSIA}+\text{O}_3_{\text{(aq)}}$  ( $f_{\text{I}}[\text{MSIA}+\text{O}_3_{\text{(aq)}}$ )), (c)  $\text{MSIA}+\text{OH}_{\text{(g)}}$  ( $f_{\text{I}}[\text{MSIA}+\text{OH}_{\text{(g)}}$ ) and (d)  $\text{MSIA}+\text{O}_3_{\text{(g)}}$  ( $f_{\text{I}}[\text{MSIA}+\text{O}_3_{\text{(g)}}$ )).

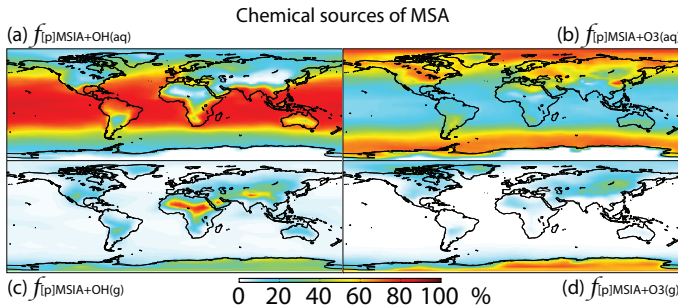
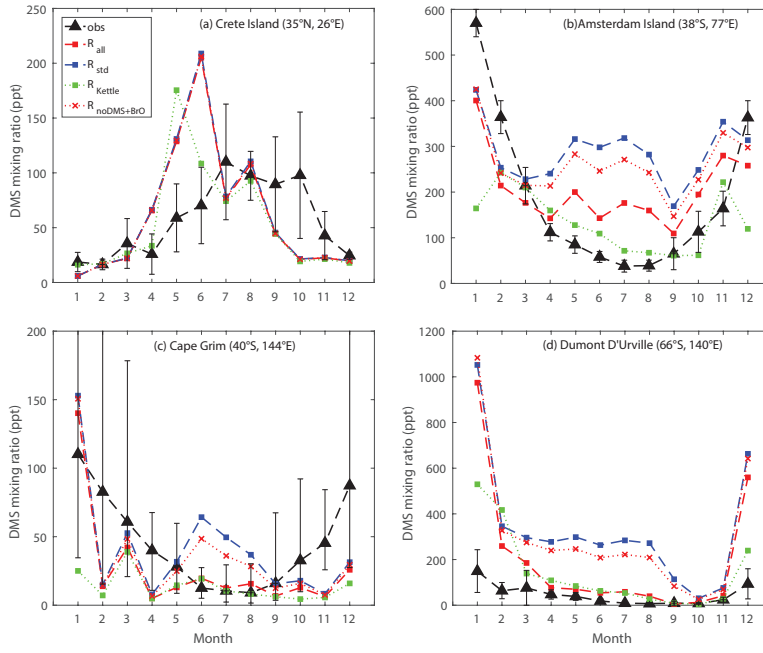


Figure 8: Global tropospheric distribution of annual-mean percentage of MSA produced in the troposphere (a) MSIA+OH<sub>(aq)</sub> ( $f_{[p]MSIA+OH(aq)}$ ), (b) MSIA+O<sub>3(aq)</sub> ( $f_{[p]MSIA+O3(aq)}$ ), (c) MSIA+OH<sub>(g)</sub> ( $f_{[p]MSIA+OH(g)}$ ) and (d) MSIA+O<sub>3(g)</sub> ( $f_{[p]MSIA+O3(g)}$ ).



5 Figure 9: Comparison between modeled and observed monthly mean surface DMS mixing ratios at (a) Crete Island (CI), (b) Amsterdam Island (AI), (c) Cape Grim (CG), and (d) Dumont D'Urville (DU) stations.

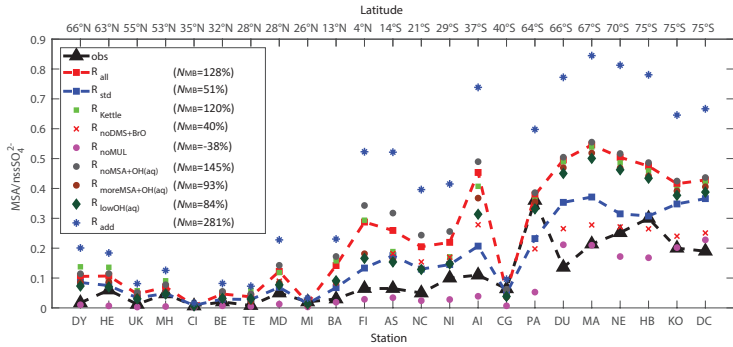


Figure 10: Comparison between modeled (nine model runs described in Table 3) and observed (obs, black triangle) annual mean surface MSA/nssSO<sub>4</sub><sup>2-</sup> ratios at 23 stations around the globe. The normalized mean bias  $N_{\text{MB}} = \frac{\sum_{i=1}^{23} (M_i - O_i)}{\sum_{i=1}^{23} O_i} \times 100\%$ , where  $M_i$  and  $O_i$  are modeled value and observed value, respectively, is shown in inset.

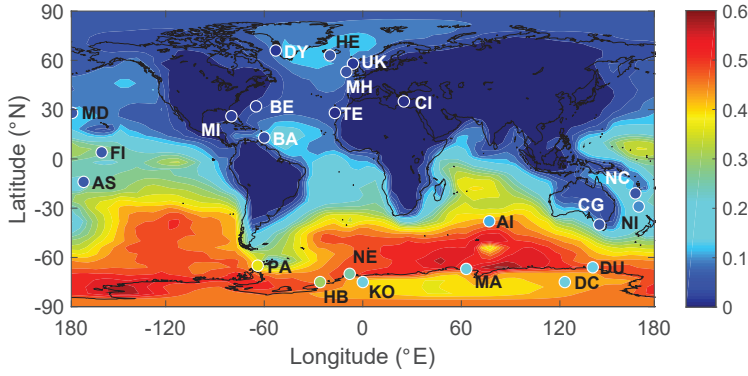


Figure 11: Global distribution of annual mean surface MSA/nssSO<sub>4</sub><sup>2-</sup> molar ratios from the full model run ( $R_{\text{all}}$ ), overplotted with observed annual mean surface MSA/nssSO<sub>4</sub><sup>2-</sup> ratios from 23 stations around the globe.

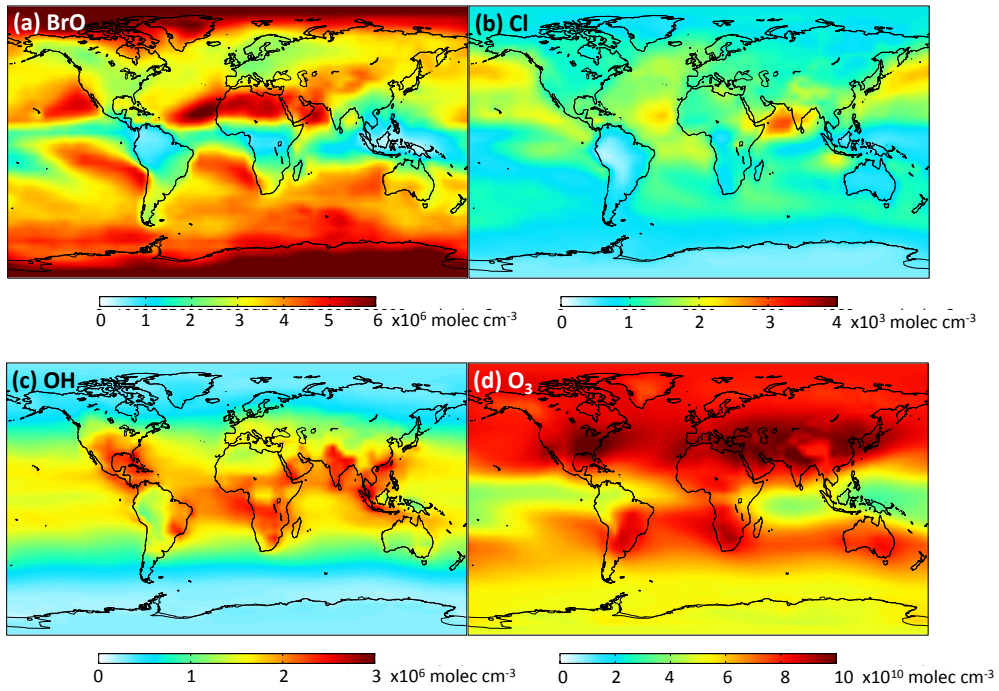


Figure 12: Global tropospheric distribution of annual-mean gas-phase (a) BrO, (b) Cl, (c) OH and (d) O<sub>3</sub> concentration.

5

10

31

**Tables**
**Table 1.** Overview of sulfur chemistry in the full model run ( $R_{\text{all}}$ ) with DMSO and MSIA intermediates and all 12 new reactions.

Gas-phase reactions	$k_{298} [\text{cm}^3 \text{s}^{-1}]$	$-\Delta E_a/\text{R} [\text{K}]$	Reference
$\text{DMS} + \text{OH} \xrightarrow{\text{abstraction}} \text{SO}_2 + \text{CH}_3\text{O}_2 + \text{CH}_2\text{O}$	$4.69 \times 10^{-12}$	-280	Burkholder et al. (2015)
$\text{DMS} + \text{OH} \xrightarrow{\text{addition}} 0.6\text{SO}_2 + 0.4\text{DMSO} + \text{CH}_3\text{O}_2^{(\text{new})}$	see note <sup>(a)</sup>		Burkholder et al. (2015); Pham et al. (1995); Spracklen et al. (2005)
$\text{DMS} + \text{NO}_3 \rightarrow \text{SO}_2 + \text{HNO}_3 + \text{CH}_3\text{O}_2 + \text{CH}_2\text{O}$	$1.13 \times 10^{-12}$	530	Burkholder et al. (2015)
$\text{DMS} + \text{BrO} \rightarrow \text{DMSO} + \text{Br}^{(\text{new})}$	$3.39 \times 10^{-13}$	950	Burkholder et al. (2015)
$\text{DMS} + \text{O}_3 \rightarrow \text{SO}_2^{(\text{new})}$	$1.00 \times 10^{-19}$	0	Burkholder et al. (2015); Du et al. (2007)
$\text{DMS} + \text{Cl} \rightarrow 0.5\text{SO}_2 + 0.5\text{DMSO} + 0.5\text{HCl} + 0.5\text{ClO}^{(\text{new})}$	$3.40 \times 10^{-10}$	0	Burkholder et al. (2015); Barns et al. (2006); IUPAC <sup>(e)</sup>
$\text{DMSO} + \text{OH} \rightarrow 0.95\text{MSIA} + 0.05\text{SO}_2^{(\text{new})}$	$8.94 \times 10^{-11}$	800	Burkholder et al. (2015); von Glasow and Crutzen (2004)
$\text{MSIA} + \text{OH} \rightarrow 0.9\text{SO}_2 + 0.1\text{MSA}^{(\text{new})}$	$9.0 \times 10^{-11}$	0	Burkholder et al. (2015); Kukui et al. (2003); Hoffmann et al. (2016); Zhu et al. (2006)
$\text{MSIA} + \text{O}_3 \rightarrow \text{MSA}^{(\text{new})}$	$2.0 \times 10^{-18}$	0	Lucas and Prinn (2002); von Glasow and Crutzen (2004)
$\text{SO}_2 + \text{OH} \xrightarrow{\text{O}_2, \text{H}_2\text{O}} \text{H}_2\text{SO}_4 + \text{HO}_2$	see note <sup>(b)</sup>		Burkholder et al. (2015)
Aqueous-phase reactions	$k_{298} [\text{M}^{-1} \text{s}^{-1}]$	$-\Delta E_a/\text{R} [\text{K}]$	Reference
$\text{DMS}_{(\text{aq})} + \text{O}_3_{(\text{aq})} \rightarrow \text{DMSO}_{(\text{aq})} + \text{O}_2_{(\text{aq})}^{(\text{new})}$	$8.61 \times 10^8$	-2600	Gershenzon et al. (2001)
$\text{DMSO}_{(\text{aq})} + \text{OH}_{(\text{aq})} \rightarrow \text{MSIA}_{(\text{aq})}^{(\text{new})}$	$6.63 \times 10^9$	-1270	Zhu et al. (2003)
$\text{MSIA}_{(\text{aq})} + \text{OH}_{(\text{aq})} \rightarrow \text{MSA}_{(\text{aq})}^{(\text{new})}$	$6.00 \times 10^9$	0	Sehested and Holcman (1996)
$\text{MSI}^- + \text{OH}_{(\text{aq})} \rightarrow \text{MSA}_{(\text{aq})}^{(\text{new})}$	$1.20 \times 10^{10}$	0	Bardouki et al. (2002)
$\text{MSIA}_{(\text{aq})} + \text{O}_3_{(\text{aq})} \rightarrow \text{MSA}_{(\text{aq})}^{(\text{new})}$	$3.50 \times 10^7$	0	Hoffmann et al. (2016)
$\text{MSI}^- + \text{O}_3_{(\text{aq})} \rightarrow \text{MS}^-^{(\text{new})}$	$2.00 \times 10^6$	0	Flyunt et al. (2001)
$\text{MSA}_{(\text{aq})} + \text{OH}_{(\text{aq})} \rightarrow \text{SO}_4^{2-}^{(\text{new})}$	$1.50 \times 10^7$	0	Hoffmann et al. (2016)
$\text{MS}^- + \text{OH}_{(\text{aq})} \rightarrow \text{SO}_4^{2-}^{(\text{new})}$	$1.29 \times 10^7$	-2630	Zhu et al. (2003)

$\text{HSO}_3^- + \text{H}_2\text{O}_{2(\text{aq})} + \text{H}^+ \rightarrow \text{SO}_4^{2-} + 2\text{H}^+ + \text{H}_2\text{O}_{(\text{aq})}$	$2.36 \times 10^{3(c)}$	-4760	Jacob (1986)
$\text{HSO}_3^- + \text{O}_{3(\text{aq})} \rightarrow \text{SO}_4^{2-} + \text{H}^+ + \text{O}_{2(\text{aq})}$	$3.20 \times 10^5$	-4830	Jacob (1986)
$\text{SO}_3^{2-} + \text{O}_{3(\text{aq})} \rightarrow \text{SO}_4^{2-} + \text{O}_{2(\text{aq})}$	$1.00 \times 10^9$	-4030	Jacob (1986)
$\text{S(IV)} + \text{O}_{2(\text{aq})} \xrightarrow{\text{Mn(II), Fe(III)}} \text{SO}_4^{2-}$	see note <sup>(d)</sup>		Martin and Good (1991)
$\text{HSO}_3^- + \text{HOBr}_{(\text{aq})} \rightarrow \text{SO}_4^{2-} + 2\text{H}^+ + \text{Br}^-$	$3.20 \times 10^9$	0	Liu(2000); Chen et al.(2016; 2017)
$\text{SO}_3^{2-} + \text{HOBr}_{(\text{aq})} \rightarrow \text{SO}_4^{2-} + \text{H}^+ + \text{Br}^-$	$5.00 \times 10^9$	0	Troy and Margerum (1991)

<sup>(new)</sup> New reaction added in the model.

<sup>(a)</sup>  $k(T, [\text{O}_2], [\text{M}]) = 8.2 \times 10^{-39} [\text{O}_2]^{53/6/T} / (1 + 1.05 \times 10^{-5} ([\text{O}_2]/[\text{M}]) e^{3644/T}) \text{ cm}^3 \text{ molecule}^{-1} \text{ s}^{-1}$ .

<sup>(b)</sup> low pressure limit:  $3.3 \times 10^{-31} (300/T)^{4.3} \text{ cm}^6 \text{ molecule}^{-2} \text{ s}^{-1}$ ; high pressure limit:  $1.6 \times 10^{-12} \text{ cm}^3 \text{ molecule}^{-1} \text{ s}^{-1}$ .

<sup>(c)</sup> Rate constant between  $\text{HSO}_3^- + \text{H}_2\text{O}_{2(\text{aq})}$  at pH=4.5.

5 <sup>(d)</sup> The metal-catalyzed sulfate production rate is calculated from the following expression:

$$-\frac{d[\text{SO}_4^{2-}]}{dt} = 750[\text{Mn(II)}][\text{S(IV)}] + 2600[\text{Fe(III)}][\text{S(IV)}] + 1.0 \times 10^{10}[\text{Mn(II)}][\text{Fe(III)}][\text{S(IV)}]$$

Detailed description about  $[\text{Mn(II)}]$  and  $[\text{Fe(III)}]$  concentrations can be found in Alexander et al. (2009).

<sup>(e)</sup> IUPAC: [http://iupac.pole-ether.fr/htdocs/datasheets/pdf/SOx13\\_Cl\\_CH3SCH3.pdf](http://iupac.pole-ether.fr/htdocs/datasheets/pdf/SOx13_Cl_CH3SCH3.pdf)

10 **Table 2.** Henry's law constant at 298 K ( $H_{X(298)}$ ), mass accommodation coefficient ( $\alpha_b$ ) and aqueous-phase diffusivity at 298 K ( $D_{l(298K)}$ ) for DMS, DMSO, MSIA and MSA, and acid dissociation constant ( $\text{pK}_a$ ) for MSIA and MSA at 298 K.

	$H_{X(298)}$ [M atm <sup>-1</sup> ]	$-\Delta H/R$ [K]	Reference	$\text{pK}_a$	Reference	$\alpha_b$	Reference	$D_{l(298K)}$ [m <sup>2</sup> s <sup>-1</sup> ]	Reference
DMS	0.56	-4480	Campolongo et al. (1999)	/	/	0.001	Zhu et al. (2006)	$1.5 \times 10^{-5}$	Saltzman et al. (1993)
DMSO	$1 \times 10^7$	-2580	Campolongo et al. (1999)	/	/	0.1	Zhu et al. (2006)	$1.0 \times 10^{-5}$	Zhu et al. (2003)
MSIA	$1 \times 10^8$	-1760	Campolongo et al. (1999)	2.28 <sup>(a)</sup>	Wudl et al. (1967)	0.1	Zhu et al. (2006)	$1.2 \times 10^{-5}$	Same as MSA
MSA	$1 \times 10^9$	-1760	Campolongo et al. (1999)	-1.86 <sup>(b)</sup>	Clarke and Woodward (1966)	0.1	Zhu et al. (2006)	$1.2 \times 10^{-5}$	Schweitzer et al. (1998)

<sup>(a)</sup>  $\text{CH}_3\text{SO}_2\text{H} \leftrightarrow \text{CH}_3\text{SO}_2^- + \text{H}^+$

<sup>(b)</sup>  $\text{CH}_3\text{SO}_3\text{H} \leftrightarrow \text{CH}_3\text{SO}_3^- + \text{H}^+$

**Table 3.** Overview of model runs.

Model run	Specification
$R_{\text{all}}$	Full model run including all reactions described in Table 1, including the DMSO and MSIA intermediates; sea surface water DMS concentration obtained from Lana et al. (2011)
$R_{\text{std}}$	Standard run which includes gas-phase oxidation of DMS by OH and $\text{NO}_3$ only, with no DMSO or MSIA intermediates
$R_{\text{Kettle}}$	$R_{\text{all}}$ ; sea surface water DMS concentration obtained from Kettle et al. (1999)
$R_{\text{noDMS+BrO}}$	$R_{\text{all}}$ ; without DMS+BrO reaction
$R_{\text{noMUL}}$	$R_{\text{all}}$ ; without multiphase oxidation of DMS, DMSO, MSIA and MSA
$R_{\text{noMSA+OH(aq)}}$	$R_{\text{all}}$ ; without MSA+OH <sub>(aq)</sub> reaction
$R_{\text{lessMSA+OH(aq)}}$	$R_{\text{all}}$ ; $k_{\text{MSA+OH(aq)}}/4.7$ (Zhu et al., 2003)
$R_{\text{lowOH(aq)}}$	$R_{\text{all}}$ ; reduce OH <sub>(aq)</sub> concentrations in cloud droplets and aerosols by a factor of 100
$R_{\text{add}}$	$R_{\text{all}}$ ; a unity yield of DMSO for the addition channel of DMS+OH reaction <sup>a</sup>
$R_{\text{10Cl}}$	$R_{\text{10Cl}}$ ; increase Cl mixing ratios by a factor of 10
$R_{\text{all\_onlyDMS}}$	$R_{\text{all}}$ ; DMS emission from the ocean is the only sulfur source
$R_{\text{std\_onlyDMS}}$	$R_{\text{std}}$ ; DMS emission from the ocean is the only sulfur source

<sup>a</sup>The product yield for the addition channel of the DMS+OH reaction is highly uncertain. Product yields of 0.6 for  $\text{SO}_2$  and 0.4 for DMSO have been commonly used in global models (Pham et al., 1995; Cosme et al., 2002; Spracklen et al., 2005; Breider et al., 2010) based on experiments described in Turnipseed et al. (1996) and Hynes et al. (1993), and is used in this study (e.g., in  $R_{\text{all}}$ ). Experiments under  $\text{NO}_x$ -free conditions suggest a DMSO yield near unity (Arsene et al., 1999; Barnes et al., 2006), as used in the sensitivity simulation  $R_{\text{add}}$ .

**Table 4.** The uncertainties of the rate constants for the 12 reactions added in the model. The uncertainty factor  $f_{298}$  means the reaction rate constant may be greater than or less than the recommended value by the factor  $f_{298}$ . Type “R”, “L” and “M” represents values obtained from “ literature reviews”, “laboratory measurements” and “modeling studies”, respectively.

Gas-phase reactions	$f_{298}$	Type	Reference
$\text{DMS} + \text{OH} \xrightarrow{\text{addition}} \dots$	1.2	R	Burkholder et al. (2015)
$\text{DMS} + \text{BrO} \rightarrow \dots$	1.3	R	Burkholder et al. (2015)
$\text{DMS} + \text{O}_3 \rightarrow \dots$	1.2	L	Du et al. (2007)
$\text{DMS} + \text{Cl} \rightarrow \dots$	1.2	R	Burkholder et al. (2015)
$\text{DMSO} + \text{OH} \rightarrow \dots$	1.2	R	Burkholder et al. (2015)
$\text{MSIA} + \text{OH} \rightarrow \dots$	1.4	R	Burkholder et al. (2015)
$\text{MSIA} + \text{O}_3 \rightarrow \dots$	1.5	M	Lucas and Prinn (2002)
Aqueous-phase reactions	$k_{298} [\text{M}^{1-n} \text{ s}^{-1}]$	Type	Reference
$\text{DMS}_{(\text{aq})} + \text{O}_3_{(\text{aq})} \rightarrow \dots$	$(8.6 \pm 8.1) \times 10^8$	L	Gershenson et al. (2001)
	$(6.1 \pm 2.4) \times 10^8$	L	Lee and Zhou (1994)
$\text{DMSO}_{(\text{g})} + \text{OH}_{(\text{aq})} \rightarrow \dots$	$(6.6 \pm 0.7) \times 10^9$	L	Zhu et al. (2003)
	$7.5 \times 10^9$	M	Hoffmann et al. (2016)
	$(4.5 \pm 0.4) \times 10^9$	L	Bardouki et al. (2002)
	$(5.4 \pm 0.3) \times 10^9$	L	Milne et al. (1989)
$\text{MSIA}_{(\text{aq})} + \text{OH}_{(\text{aq})} \rightarrow \dots$	$(6.0 \pm 1.0) \times 10^9$	L	Sehested and Holzman (1996)
$\text{MSI}^- + \text{OH}_{(\text{aq})} \rightarrow \dots$	$(1.2 \pm 0.2) \times 10^{10}$	L	Bardouki et al. (2002)
	$7.7 \times 10^9$	M	Zhu et al. (2006)
$\text{MSIA} + \text{O}_3_{(\text{aq})} \rightarrow \dots$	$3.5 \times 10^7$	M	Hoffmann et al. (2016)
$\text{MSI}^- + \text{O}_3_{(\text{aq})} \rightarrow \dots$	$2.0 \times 10^6$	L	Flyunt et al. (2001)
$\text{MSA}_{(\text{aq})} + \text{OH}_{(\text{aq})} \rightarrow \dots$	$1.5 \times 10^7$	M	Hoffmann et al. (2016)
$\text{MS}^- + \text{OH}_{(\text{aq})} \rightarrow \dots$	$(1.3 \pm 0.1) \times 10^7$	L	Zhu et al. (2003)
	$(6.1 \pm 1.1) \times 10^7$	L	Milne et al. (1989)

**Table 5.** The locations of the 23 stations that provide annual-mean MSA/nssSO<sub>4</sub><sup>2-</sup> observations.

Station name	Location	Station name	Location
Dye (DI)	66°N, 53°E	American Samoa (AS)	14°S, 170°W
Heimaey (HE)	63°N, 20°W	New Caledonia (NC)	21°S, 166°E
United Kingdom (UK)	58°N, 6°W	Norfolk Island (NI)	29°S, 168°E
Mace Head (MH)	53°N, 10°W	Amsterdam Island (AI)	38°S, 77°E
Crete Island (CI)	35°N, 25°E	Cape Grim (CG)	40°S, 144°E
Bermuda (BE)	32°N, 65°W	Palmer (PA)	65°S, 64°W
Tenerife (TE)	28°N, 17°W	Dumont D'Urville (DU)	66°S, 140°E
Midway Island (MD)	28°N, 177°W	Mawson (MA)	67°S, 63°E
Miami (MI)	26°N, 80°W	Neumayer (NE)	70°S, 8°W
Barbados (BA)	13°N, 60°W	Halley Bay (HB)	75°S, 26°W
Fanning Island (FI)	4°N, 159°W	Kohnen (KO)	75°S, 0°E
		Dome C (DC)	75°S, 123°E